ANNUAL REPORT

DRA

FLUID DYNAMICS IN FLEXIBLE TUBES: AN APPLICATION TO THE STUDY OF THE PULMONARY CIRCULATION

PREPARED FOR: National Aeronautics and Space Administration
Washington, D.C. 20546

Contract No.: NASW-2138

PREPARED BY: Dr. N.R. Kuchar
Environmental Sciences Laboratory
Re-Entry and Environmental Systems Division
General Electric Company
Philadelphia, Pennsylvania 19101

December 31, 1971

GENERAL ELECTRIC
Re-entry & Environmental Systems Division

ANNUAL REPORT

FLUID DYNAMICS IN FLEXIBLE TUBES: AN APPLICATION TO THE STUDY OF THE PULMONARY CIRCULATION

PREPARED FOR: National Aeronautics and Space Administration
Washington, D.C. 20546

Contract No.: NASW-2138

PREPARED BY: Dr. N.R. Kuchar
Environmental Sciences Laboratory
Re-Entry and Environmental Systems Division
General Electric Company
Philadelphia, Pennsylvania 19101

December 31, 1971

TABLE OF CONTENTS

		PAGE
List of Figures		iii
Nomenclature		v
Abstract		vi
I.	Introduction	1
II.	The Pulmonary Circulation	5
III.	Mathematical Modelling of the Pulmonary Circulation	15
	A. Theoretical Background	15
	B. The Mathematical Model and Its Solution	25
IV.	Simulations of Pulmonary Circulation Dynamics	38
	A. The Range of Environmental and Pathological Conditions Simulated	38
	B. Results of the Simulations	42
V.	Conclusions	93
	References	95

LIST OF FIGURES

		PAGE
1.	Schematic Diagram of the Cardiovascular System	5
2.	Lobes of the Lungs (Lateral Views)	6
3.	Typical Variation of Pulmonary Vascular Resistance with Mean Transmural Pressure	8
4.	Typical Relationship Between Main Pulmonary Arterial Pressure and Pulmonary Blood Flow Rate (Left Atrial and External Pressures Normal)	9
5.	Pressures in the Main Pulmonary Artery and Left Atrium of Man, Over One Pulse Cycle: (a) Physiological Data, (b) Functions Used in Model	12
6.	Alveolar and Intrathoracic Pressures in Man, Over One Respiratory Cycle: (a) Physiological Data, (b) Functions Used in Model	13
7.	An Analogous Electrical Circuit for Blood Flow in a Segment of a Vessel	20
8.	The Pulmonary Circulation Model in Electrical Analog Form	26
9.	Variation of Total Pulmonary Vascular Resistance With Transmural Pressure	28
10.	Parameter Values Used for the Simulation of the Control State	30
11.	Flow Chart for the Control of Mean Pulmonary Blood Flow Rate by Adjustment of Mean Pulmonary Arterial Pressure.	33
12.	Analog Computer Circuit for a Vascular Segment	35
13.	Simulation of the Control State - Pressures	43
14.	Simulation of the Control State - Flow Rates	45
15.	Effect of Pulmonary Blood Flow Rate on Pressure in the Main Pulmonary Artery	49
16.	Effect of Left Atrial Pressure on Pulmonary Arterial Pressure	51

PAGE

17. Model Prediction of the Effect of Venous Pressure on Pulmonary Blood Flow Rate 53

18. Model Prediction of the Effect of Alveolar Pressure on Pulmonary Blood Flow Rate 54

19. Simulations of the Effects of Inertial Loadings and Vascular Deconditioning - Pressures 61

20. Simulations of the Effects of Inertial Loadings and Vascular Deconditioning - Volumes and Flow Rates 62

21. Model Prediction of Topographical Distribution of Blood Flow in the Lung (1 G_z) 64

22. Simulation of Effects of Exercise 67

23. Simulation of Effects of Hypoxia 70

24. Simulations of the Effects of Pulmonary Embolism - Pressures and Volumes 73

25. Simulations of the Effects of Pulmonary Embolism - Blood Flow Rates 74

26. Simulation of Excision of the Right Lung - Pressures and Volumes 77

27. Simulation of Excision of the Right Lung - Blood Flow Rates 78

28. Simulation of Circulatory Shock 80

29. Simulation of Mitral Stenosis 83

30. Simulations of Effects of Atrial Septal Defects, With and Without Reactive Vascular Changes 87

31. Simulations of the Effects of Emphysema and Interstitial Fibrosis During Rest and Exercise - Pressures 90

32. Simulations of the Effects of Emphysema and Interstitial Fibrosis During Rest and Exercise - Volumes and Flow Rates 91

NOMENCLATURE

A	amplitude of pressure
a	unstressed internal vessel radius
C	compliance or capacitance
c	wave propagation velocity
D	distance from base of lung
E	Young's modulus of vessel wall
f_c	cutoff frequency of filter circuit
G	perivascular or hydrostatic pressures
G_z	terrestrial gravitational acceleration, acting in caudal direction
h	vessel wall thickness
J_n	Bessel function of the first kind and order n
j	$\sqrt{-1}$
K	a function of α , see Equation (7)
L	inertance or inductance
ℓ	length of vessel segment
P	pressure
Q	blood flow rate
R	viscous or electrical resistance
r	radial coordinate
t	time
u	axial velocity component
V	volume
v	radial velocity component
x	axial coordinate
Z_ℓ'	longitudinal impedance per unit length
Z_t'	transverse impedance times length
Z_0	characteristic impedance of a vascular segment
α	dimensionless flow parameter, $\alpha = a\sqrt{\rho\omega/\mu}$
η	radial component of vessel wall displacement
μ	dynamic viscosity of blood
ξ	axial component of vessel wall displacement
ρ	density of blood
σ	Poisson ratio of vessel wall
ω	angular frequency

Superscripts

'	(prime) per unit length
-	(bar) mean
*	(asterisk) set point value

Subscripts

e	external or perivascular
i	inlet of segment
o	outlet of segment
alv	alveolar
art	large arteries
ven	large veins

for numbered subscripts on C,G,L,P,Q,R,V, see Figure 8.

ABSTRACT

Based on an analysis of unsteady, viscous flow through distensible tubes, a lumped-parameter model for the dynamics of blood flow through the pulmonary vascular bed has been developed. The model is non-linear, incorporating the variation of flow resistance with transmural pressure. Solved using a hybrid computer, the model yields information concerning the time-dependent behavior of blood pressures, flow rates, and volumes in each important class of vessels in each lobe of each lung in terms of the important physical and environmental parameters. Simulations of twenty abnormal or pathological situations of interest in environmental physiology and clinical medicine were performed. The model predictions agree well with physiological data.

I. INTRODUCTION

Considered from a mechanical standpoint, the cardiovascular system consists of a complex network of distensible tubes through which a viscous liquid is driven by the pumping action of the heart. Attempts at understanding the function of this system by the application of physical principles began about two centuries ago and include work by L. Euler, Th. Young, E.H. Weber, J.L.M. Poiseuille, and others well known in the physical and engineering sciences[1,2]. In recent years, the effort to apply fluid and solid mechanics to the study of the circulation has been greatly intensified. The basic work of Womersley[3] on the linear theory of pulsatile flow and wave propagation in arteries has now been broadened to include effects due to more complex vessel properties[4-6], entrance regimes[7,8], nonlinearities[9,10], and other phenomena. In addition, models for blood flow in veins[11] and capillaries[12-16] have been developed recently. These studies have yielded much information concerning pulse propagation, blood pressure-flow relationships, blood velocity distributions, and wall deformations in individual vessels.

This knowledge is important and has yielded insight into some of the physical mechanisms of the circulation. Clinically, work of this type can be applied directly to the study of some diseased conditions such as stenoses, aneurysms, and local atherosclerosis. However, from the standpoints of the

physiologist concerned with cardiovascular performance in abnormal environments and the clinician concerned with the effects of diseases, the blood flow in entire organs, rather than in individual vessels, is often of greater significance. It is clear that if mathematical modeling of blood flow is to be of maximum use to medicine and physiology, techniques which describe blood flow in vascular beds, and yet are consistent with the models of flow in individual vessels, must be developed. This report describes a study in which such a technique was developed and applied to a particular vascular bed - the pulmonary circulation.

The primary function of the lungs is to transport oxygen to the blood and remove carbon dioxide. Efficient operation of this system requires adequate flow and distribution of both air in the respiratory tree (ventilation) and blood in the pulmonary vascular bed (perfusion). Because of its important role in one of the body's most vital processes, the pulmonary circulation has been the subject of much interest.

One aspect of recent pulmonary research has been concerned with the normal lung functioning in an abnormal environment. Man's explorations into space and the oceans have opened questions concerning the behavior of the lungs under conditions of high inertial loading, weightlessness, vascular deconditioning, or altered alveolar pressure. In particular, the pulmonary cir-

culation, which is a highly distensible system operating at a relatively low pressure level, can be strongly affected by changes in pressures and vessel tone brought about by abnormal environments. It is important to determine the influence of environmental stresses on the dynamics of blood flow in the lungs and the movement of body fluids across the respiratory membrane. However, instrumentation problems and difficulties in maintaining subjects in the abnormal environments for long periods of time make this area of environmental physiology difficult and costly to study experimentally. Mathematical models would be useful to provide preliminary data and guide future experimental research.

The problem of the pathological lung operating in a normal environment is also of great importance. The incidence of several primary pulmonary diseases, including emphysema, asthma, and lung cancer, has been increasing. Although these diseases mainly affect the bronchial side of the lung, they have important secondary effects on the pulmonary circulation. Pulmonary blood flow is also subject to conditions caused by malfunctions in other organs, such as obstructions due to migrating emboli and alterations in pulmonary vascular impedance and blood flow due to heart defects. New approaches are needed to diagnose these pathological conditions and to understand their influence on pulmonary function; mathematical models can aid in these endeavors.

The research described herein represents the second phase of a program directed toward the modelling of the dynamics of blood flow in the lungs. The broad goals of this research have been the synthesis of a mathematical model of the pulmonary circulation and the use of this model to study the effects of abnormal environments and pathological conditions on the functioning of this vascular bed. The first phase of this work, described in a previous report[17], was primarily concerned with model development. This included determination of the model configuration, derivation of the mathematical relationships which describe the blood pressure-flow relationships, and model validation by means of associated animal experiments. The present phase has been directed toward refinement of the model and its application to the simulation of a wide variety of environmental and pathological conditions of current interest in physiology and medicine.

II. THE PULMONARY CIRCULATION

The primary function of the cardiovascular system is to transport nutrients and oxygen to, and remove carbon dioxide and other metabolic products from, the active tissues of the body. The transport medium is blood, and this fluid is pumped around a closed path by the heart (Figure 1). The heart itself consists of two pumps, left and right, each having a reservoir (atrium) and an active pumping element (ventricle).

The left heart pumps blood rich in oxygen through the arteries to the systemic circulation, which perfuses the metabolizing organs. From these organs, blood depleted in oxygen but rich in carbon dioxide is returned to right heart by the systemic veins.

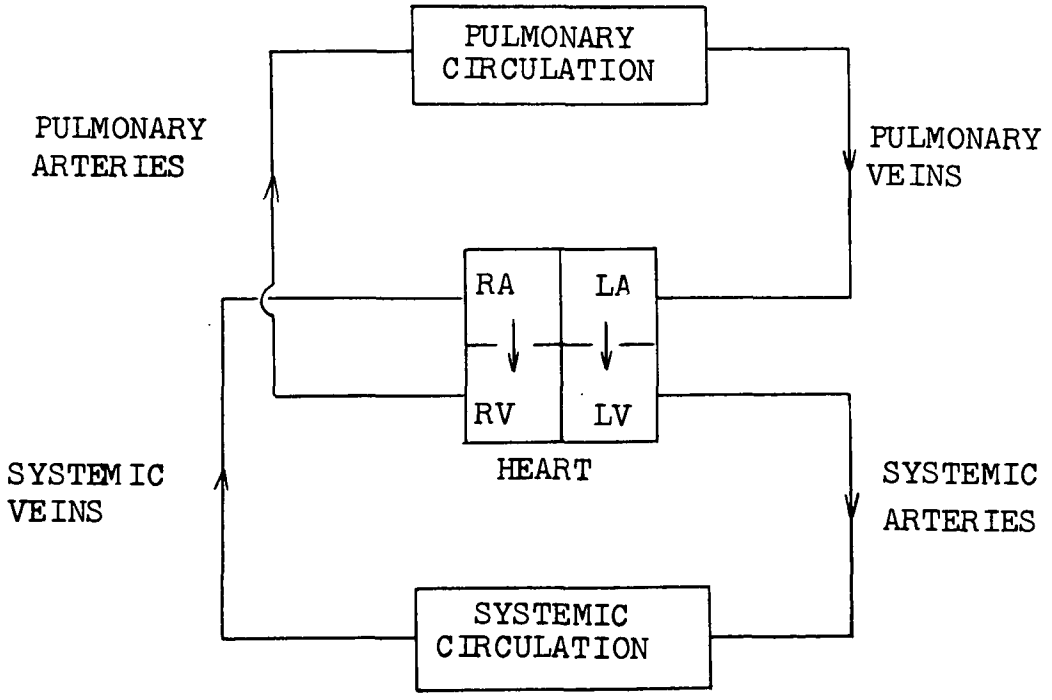

FIGURE 1. SCHEMATIC DIAGRAM OF THE CARDIOVASCULAR SYSTEM

In turn, this blood is pumped by the right heart into the pulmonary circulation. Here, in the lungs, the blood is brought into close proximity with inhaled air in the alveoli or air sacs. By diffusion across the thin separating membrane, carbon dioxide is transferred out of, and oxygen into, the blood. From the lungs, the blood flows back to the left heart, thus completing the path. In addition to its gas exchange function, the pulmonary circulation acts as a filter for small circulating clots and other emboli and serves as an additional blood reservoir for the left heart.

The anatomy or morphology of the pulmonary vascular bed is fairly well known[18-21]. Beginning at the right ventricle, blood passes through the pulmonary valve into the main pulmonary artery, a short (4 cm)[22], large diameter (3 to 4 cm)[23] vessel which divides into two branches, the left and right pulmonary arteries; these supply blood to the left and right lungs.

Each pulmonary artery itself divides into the lobar arteries, each of which perfuses a lobe of the lung. Lobes are major divisions of the lung, separated by deep fissures. In man, the left lung has two lobes, upper and lower, while the right has three, upper, middle, and lower (Figure 2).

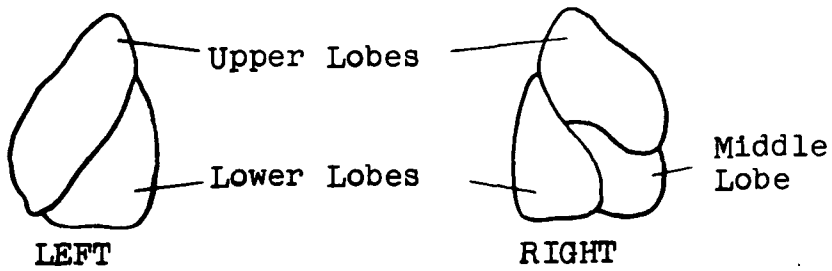

FIGURE 2. LOBES OF THE LUNGS (LATERAL VIEWS). FROM [24].

The vascular beds in each lobe are generally separate from one another. Each consists of a highly branching network of arteries, precapillaries (100 to 1000 microns diameter), arterioles (50 microns diameter), capillaries (10 to 14 microns length, 7 to 9 microns diameter, 280 billion total number), venules (collecting vessels, the size of precapillaries), and veins[25]. About 28 generations of dichotomous branchings occur between the main pulmonary artery and the smallest capillaries[19]. The capillaries themselves form a dense "sheet" of interconnecting passages in each interalveolar septum[20]. The lobar vascular beds finally coalesce into large lobar veins; generally, four of these veins empty into the left atrium[18].

Much is known about the basic physiology of the pulmonary circulation[22, 25-30]. Of particular interest is the means by which blood flow through this vascular bed is regulated. Extrinsic regulation, due to neural stimulation, probably has little importance in the pulmonary circulation[22]. Some active intrinsic control (active autoregulation) exists, which tends to shunt blood away from poorly ventilated alveoli,[22, 31] but the regulation of the pulmonary circulation is largely by passive intrinsic means. That is, the vascular bed generally acts as a passive mechanical system which responds to the level of transmural pressure (internal minus external pressure on the vessels). This response may be due to vessel distensibility, which would cause the vessels to dilate with increasing transmural

pressure and constrict with decreasing transmural pressure, or to recruitment, the opening up of additional parallel paths for perfusion as the transmural pressure rises above the critical opening pressure of the local capillaries; possibly both mechanisms play roles in the overall regulation of the pulmonary circulation.

The resistance to blood flow through the vascular bed is defined as the ratio of the mean driving pressure (main pulmonary arterial pressure minus left atrial pressure) to the mean blood flow rate. Since resistance to flow through a system of conduits depends strongly on the total cross-sectional area for flow, the vascular resistance of the pulmonary circulation is a function of the transmural pressure (Figure 3), being high when this pressure

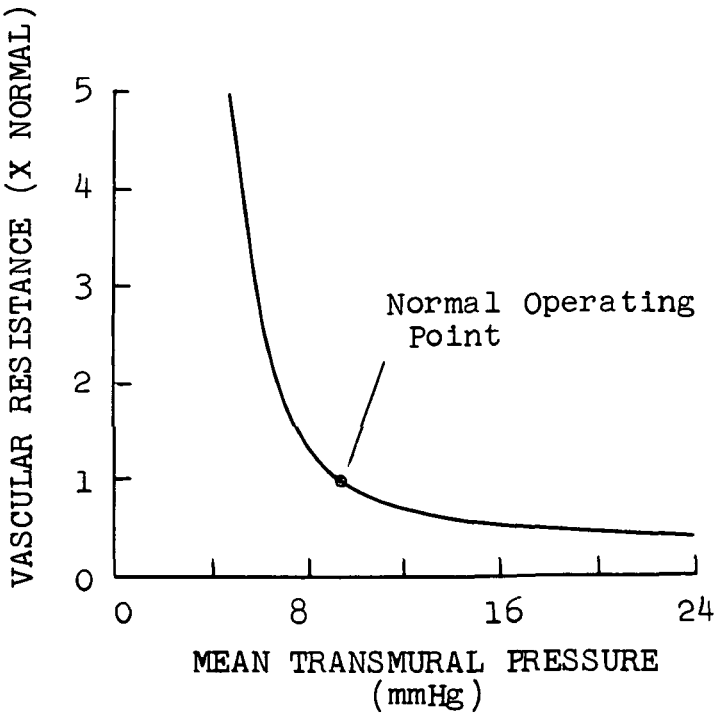

FIGURE 3. TYPICAL VARIATION OF PULMONARY VASCULAR RESISTANCE WITH MEAN TRANSMURAL PRESSURE.

is low and decreasing as this pressure increases, thus either dilating the vessels or causing additional parallel flow paths to open. The variability of the resistance makes the pulmonary circulation non-linear; that is, the blood flow rate is not linearly related to the driving pressure, as would be the case for laminar flow through a rigid system. It also makes it possible for normal lungs to accommodate large increases in blood flow (e.g., during exercise) with only small increases in pulmonary arterial pressure; this is illustrated in Figure 4, where the behavior of a rigid system is also shown for comparison.

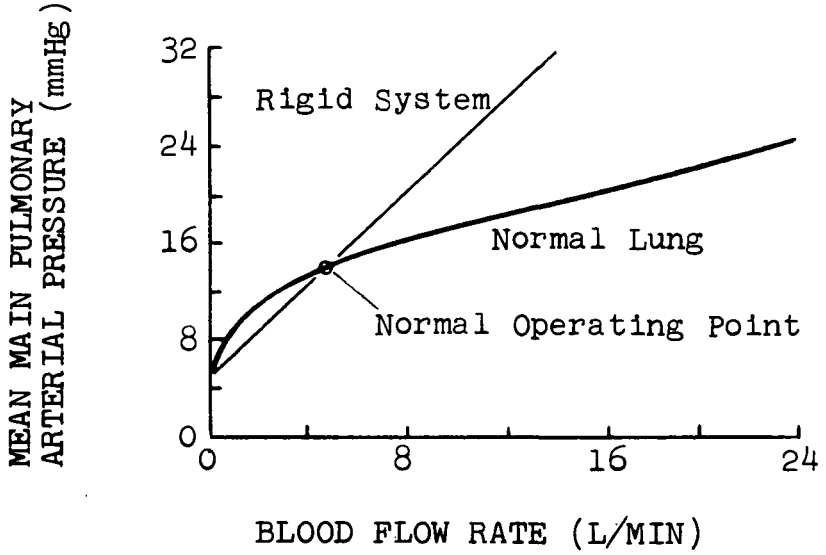

FIGURE 4. TYPICAL RELATIONSHIP BETWEEN MAIN PULMONARY ARTERIAL PRESSURE AND PULMONARY BLOOD FLOW RATE (LEFT ATRIAL AND EXTERNAL PRESSURES NORMAL).

Thus, the dynamics of the pulmonary circulation is related to both the driving pressure and the transmural pressure. In turn, these pressures depend on main pulmonary arterial and left atrial pressures (which determine the driving pressure and the level of the internal pressure in the vessels) as well as on the intrathoracic and alveolar pressures (which are the external pressures which act on the vessels); the importance of these four pressures has been established by a large number of physiological experiments[32-42].

Main pulmonary arterial pressure in normal subjects resting supine, as measured by right heart catheterization, generally has a systolic (peak) value of about 20 mmHg, a diastolic (minimum) value of about 10 mmHg, and a mean of about 14 mmHg[28, 29]; these levels are only about one-sixth the magnitudes in the aorta, the largest vessel in the systemic circulation. Left atrial pressure, which is the "back pressure" of the pulmonary circulation, fluctuates with various events in the left heart; it generally has systolic, diastolic, and mean values of 7, 3, and 5 mmHg, respectively, in normal subjects at rest. Another internal pressure capable of being measured by catheterization is the so-called arterial wedge pressure. This is measured after advancing a cardiac catheter into the pulmonary arterial branches until it occludes a small branch, blocking flow; the pressure measured then presumably approximates the pressure in the first pulmonary vein in which flow still persists by means of some parallel path.

Arterial wedge pressures generally have mean values of between 6 and 9 mmHg,[26, 28] which are slightly higher than those measured in the left atrium. Typical behavior of main pulmonary arterial and left atrial pressures over one pulse cycle is shown in Figure 5 (a).

Intrathoracic pressure is approximately the pressure on the outside of the main, left, and right pulmonary arteries. The other vessels, located deeper into the lung tissue, are acted upon by an external pressure approximately equal to alveolar pressure. Both intrathoracic and alveolar pressures fluctuate with the respiration cycle. Whereas alveolar pressure is always close to zero for normal subjects at rest, intrathoracic pressure is normally always negative, lying between about -4 and -8 mmHg, with respect to atmospheric pressure, Figure 6 (a)[44, 45].

Total blood flow rate through the pulmonary circulation is normally the same as that through the systemic circulation, about 5 liters per minute for a subject at rest. About 55% of this flow goes to the right lung in a normal supine subject[26]. The distribution to the various lobes is likewise uneven, and is greatly influenced by hydrostatic pressure heads (which alter the local transmural pressures), both in a normal 1g field and at higher inertial loadings[46-51]. The distance between the apical and diaphragmatic ends of the lung is about 25 to 30 cm, so that, in a 1g field the maximum difference in hydrostatic pressures in

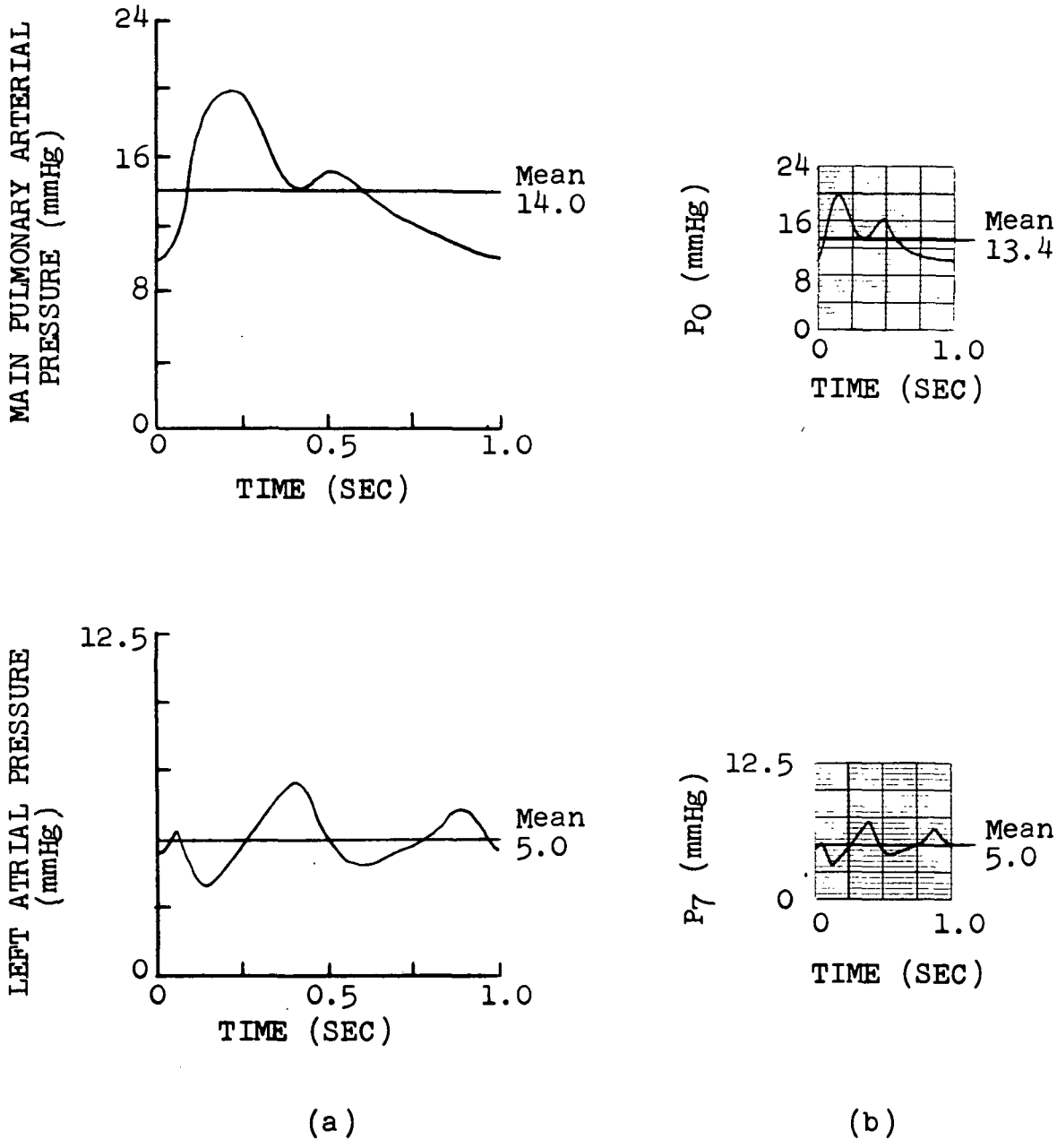

FIGURE 5. PRESSURES IN THE MAIN PULMONARY ARTERY AND LEFT ATRIUM OF MAN, OVER ONE PULSE CYCLE: (a) PHYSIOLOGICAL DATA[26, 43], (b) FUNCTIONS USED IN MODEL.

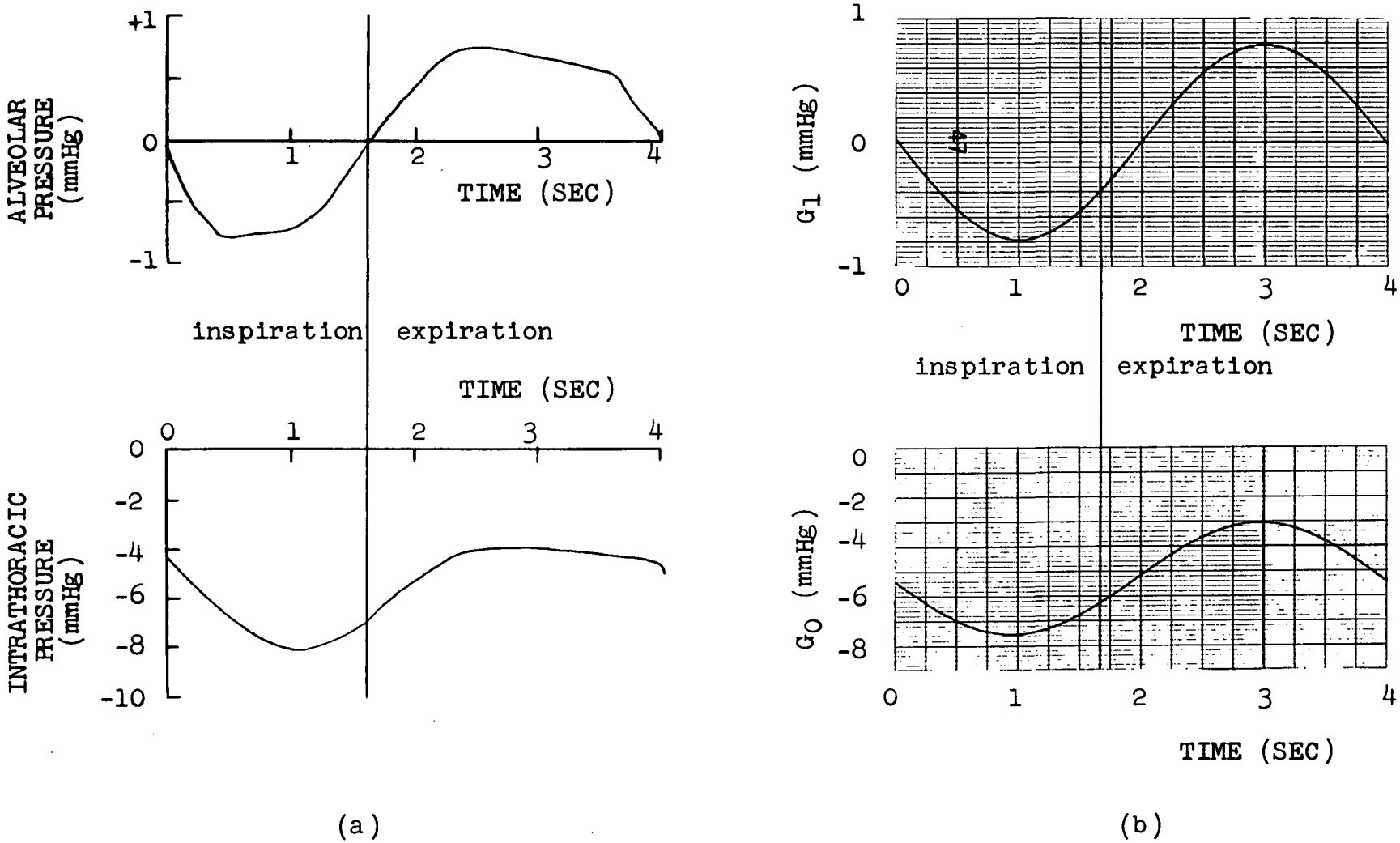

FIGURE 6. ALVEOLAR AND INTRATHORACIC PRESSURES IN MAN, OVER ONE RESPIRATORY CYCLE: (a) PHYSIOLOGICAL DATA[44, 45], (b) FUNCTIONS USED IN MODEL.

the lung is in the range of 20 mmHg, a figure equivalent to the peak pressure produced by the right ventricle.

Pathological conditions can greatly alter the dynamics of the pulmonary circulation. The most important disturbance is the elevation of arterial blood pressure within the pulmonary vascular bed (pulmonary hypertension), which can impose a greater work load on the right ventricle, causing its hypertrophy and failure. The principal cause of pulmonary hypertension is a chronic increase in resistance to blood flow, which requires elevation of the arterial pressure in order to pump even the usual cardiac output at rest through the vascular bed. The increased resistance may be due to a variety of pathological mechanisms, including vessel blockage (obstructive hypertension); vascular spasm (vasoconstrictive hypertension); destruction of parts of the vascular bed by disease (obliterative hypertension); increased blood flow through the pulmonary circulation due to intracardiac or intervascular shunts (hyperkinetic hypertension); and pressure transmitted backward from the left atrium (passive hypertension)[52]. Many diseases can produce one or more of these basic mechanisms of pulmonary hypertension.

III. MATHEMATICAL MODELLING OF THE PULMONARY CIRCULATION

A. Theoretical Background

The mechanics of blood flow can be modelled by several techniques, representing different levels of sophistication. The most detailed description can be gained by considering the vascular bed to be a distributed-parameter system. Here, the relevant mechanical parameters such as blood and vessel densities, blood viscosity, and vessel elasticity are assumed to be continuously distributed over finite volumes in space, as, indeed, they actually are. The motions of the system are then described by the field equations of fluid and solid mechanics[53], a set of partial differential equations in three space variables and time. Solution of these equations, with appropriate boundary and initial conditions, yields the continuous spatial and temporal distributions of blood velocity, blood pressure, and vessel wall displacements and stresses.

Although this technique is very powerful, it is practical only for the description of local areas in a vascular bed, such as the flow of blood through a single artery[3-8] or the deformation of a single vessel[54]. As an example, Womersley's[3] field equations for the flow of blood in a segment of an artery consist of a momentum equation for the axial direction (Newton's Second Law),

$$\frac{\partial P}{\partial x} = -\rho \frac{\partial u}{\partial t} + \mu \frac{1}{r} \frac{\partial}{\partial r} \left(r \frac{\partial u}{\partial r} \right) \qquad (1)$$

a similar equation for the radial direction, and a continuity equation (conservation of mass),

$$\frac{\partial u}{\partial x} = -\frac{1}{r} \frac{\partial}{\partial r} (rv). \qquad (2)$$

Here P is the blood pressure, u and v the axial and radial components of blood velocity, x and r the axial and radial coordinates, t time, and ρ and μ the blood density and dynamic viscosity. These equations assume that blood is an incompressible Newtonian fluid, the flow is axisymmetric, and that convective inertia and axial viscous stresses are negligible. In addition, Womersley used two equations from the theory of thin shells to describe the radial and axial vessel wall displacements, η and ξ, in terms of the pressure and viscous shear stresses exerted on the wall by the flowing blood. Boundary conditions equated the blood and wall velocities at the interface, which was assumed to be at the unstressed internal vessel radius a,

$$u = \frac{\partial \xi}{\partial t} \quad , \quad v = \frac{\partial \eta}{\partial t} \quad \text{at } r = a. \tag{3}$$

For motions periodic in time, the equations admit solutions having the form of traveling waves. If the pressure is of the form

$$P = A \exp \left[j\omega \, (t - x/c) \right] \tag{4}$$

where ω is the angular frequency, c the complex wave velocity, and the reference pressure is that on the outside of the vessel (perivascular pressure), then the axial velocity distribution is given by

$$u = (A/\rho c) \left[1 + B \, \frac{J_0(j^{3/2} \alpha \, r/a)}{J_0(j^{3/2} \alpha)} \right] \exp \left[j\omega(t-x/c) \right] \tag{5}$$

where $\alpha \equiv a\sqrt{\rho\omega/\mu}$ and B is a constant that depends on α and the Poisson ratio of the vessel wall σ. For a "stiff" axial constraint on the vessel due to external tissue attachments and an incompressible vessel material ($\sigma = 0.5$), both of which are quite realistic assumptions, B is equal to -1.

The complex wave velocity c is given by (again, for an incompressible wall material)

$$c = (2Eh\ K/3\rho a)^{\frac{1}{2}} \tag{6}$$

where K, defined by

$$K = 1 - \frac{2J_1(j^{3/2}\alpha)}{j^{3/2}\alpha J_0(j^{3/2}\alpha)} \tag{7}$$

is a complex function of the parameter α, while E is the Young's modulus of the wall and h is its thickness (assumed to be small compared to the radius a). For large values of α (i.e., high frequency or low viscosity), K approaches a real value of unity, while as α approaches zero (very low frequency or high viscosity), K approaches a purely imaginary function,

$$\begin{aligned} K &\to 1 \quad \text{as} \quad \alpha \to \infty \\ K &\to j\alpha^2/8 \ \text{as} \ \alpha \to 0. \end{aligned} \tag{8}$$

The flow rate Q, defined by

$$Q \equiv \int_0^a 2\pi r u dr \tag{9}$$

is then

$$Q = (\pi a^2 A\ K/\rho c) \exp\left[j\omega(t - x/c)\right]. \tag{10}$$

Defining the longitudinal impedance per unit length Z_ℓ' and transverse impedance times length Z_t' by

$$\begin{aligned} Z_\ell' &= -(\partial P/\partial x)/Q \\ Z_t' &= -P/(\partial Q/\partial x) \end{aligned} \tag{11}$$

it follows from Equations (4), (6), and (10) that

$$\begin{aligned} Z_\ell' &= j\omega\rho/\pi a^2 K = j\omega L' + R' \\ Z_t' &= 2Eh/3\pi\, j\omega a^3 = 1/j\omega C'. \end{aligned} \tag{12}$$

where L', R', and C' are the inertance, resistance, and compliance (all per unit vessel length), which are measures of the system's inertial, viscous, and elastic properties. It should be noted that L' and R' are functions of the parameter α (i.e., frequency); however, from Equation (8) it follows that the longitudinal impedance per unit length becomes purely inertial in character when α is very large,

$$Z_\ell' \to j\omega L'(\infty) = j\omega\rho/\pi a^2 \quad \text{as} \quad \alpha \to \infty \tag{13}$$

while it becomes purely resistive as α approaches zero,

$$Z_\ell' \to R'(0) = 8\mu/\pi a^4 \quad \text{as} \quad \alpha \to 0; \tag{14}$$

the latter is just the resistance per unit length in a Poiseuille flow. The compliance C' is independent of frequency,

$$C' = 3\pi a^3/2Eh. \tag{15}$$

From Equations (11) and (12), the relationships between pressure, flow rate, and their gradients are

$$\begin{aligned} -\frac{\partial P}{\partial x} &= (j\omega L' + R')\, Q \\ -\frac{\partial Q}{\partial x} &= (j\omega C')\, P. \end{aligned} \tag{16}$$

These expressions may be formally written as

$$
\begin{aligned}
-\frac{\partial P}{\partial x} &= L' \frac{\partial Q}{\partial t} + R' Q \\
-\frac{\partial Q}{\partial x} &= C' \frac{\partial P}{\partial t}
\end{aligned}
\tag{17}
$$

which are in the so-called transmission-line form; that is, if P is identified with voltage, Q with current, and L', R', and C' with inductance, electrical resistance, and capacitance to ground (all per unit length), then these equations are identical to those for the flow of electricity in a long transmission line, when the conductance to ground is zero. These equations still represent a distributed-parameter description of blood flow, but they are less sophisticated than the field equation description since here the parameters are distributed only along the length of the vessel, with radial variations ignored; furthermore, these equations describe total cross-sectional flow rate rather than the details of the velocity distribution.

It is now possible to transfer to a lumped-parameter description by considering finite axial segments of length ℓ. This is useful in synthesizing a model of a complex system of branched tubes, each of which has only a finite length. Denoting quantities at the inlet and outlet of the finite segment by the subscripts i and o, external conditions by the subscript e, and referring pressures to the atmospheric level rather than to the external (perivascular) level, Equations (17) become, using the difference form in the axial direction,

$$
\begin{aligned}
P_i - P_o &= L \frac{dQ}{dt} + R Q \\
Q_i - Q_o &= C \frac{d}{dt} (P - P_e)
\end{aligned}
\tag{18}
$$

where L, R, and C are merely L', R', and C', respectively, multiplied by the segment length ℓ. On the right-hand side the positions within the segment to which P and Q are referred are as yet undefined. Equations (18) are ordinary differential equations analogous to those describing a time-varying electrical circuit with series inductance L and resistance R and shunt capacitance C, if, again, pressure and flow rate are identified with voltage and current, respectively (in this analogy, volume is analogous to electrical charge). A number of arrangements of the circuit parameters (e.g., T-networks, π-networks, L-networks[55]) are possible within the framework of Equations (18); somewhat arbitrarily, in the present model an L-network (Figure 7) with the capacitance located downstream of the inductance and resistance is used (theoretically, the use of π-networks has some advantages,[56] but the improvement is relatively small[1]).

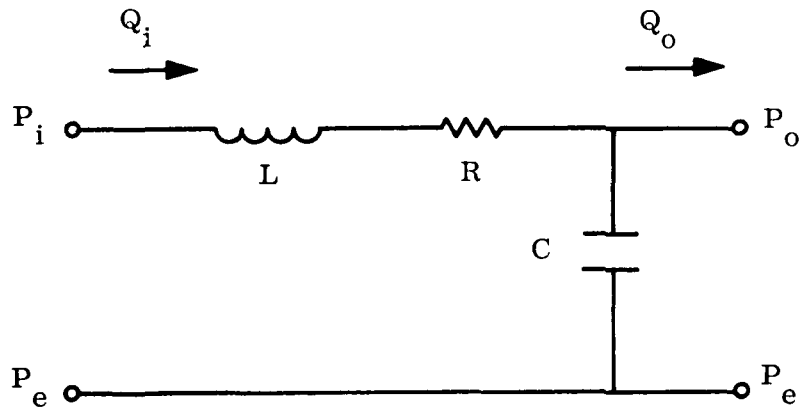

FIGURE 7. AN ANALOGOUS ELECTRICAL CIRCUIT FOR BLOOD FLOW IN A SEGMENT OF A VESSEL.

Then, Equations (18) become

$$P_i - P_o = L \frac{dQ_i}{dt} + RQ_i$$
$$Q_i - Q_o = C \frac{d}{dt} (P_o - P_e) \tag{19}$$

or, in integrated form,

$$Q_i = \frac{1}{L} \int (P_i - P_o - RQ_i)\, dt$$
$$P_o = P_e + \frac{1}{C} \int (Q_i - Q_o)\, dt. \tag{20}$$

The stored blood volume V, above a reference value when P_o is equal to P_e, is just

$$V = \int (Q_i - Q_o)\, dt = C (P_o - P_e). \tag{21}$$

Since Equations (20) contain five unknowns, it is clear that three of the quantities (e.g., P_i, P_e, and Q_o) must be specified in order to obtain unique solutions for the other two (e.g., P_o and Q_i).

It should be noted that the inertance and resistance are, strictly speaking, functions of the parameter $\alpha \equiv a\sqrt{\rho\omega/\mu}$ (see Equations (7) and (12)). Elaborate correction networks to the basic L-R-C circuit (Figure 7) have been developed[1, 57] to account for this frequency dependence, but it has been found that no large deviations occur if constant values for L and R are used, even when these values are based on the contradictory assumptions of very large α for L and very small α for R, Equations (13) and (14).

A circuit having the configuration shown in Figure 7 is known as a low-pass filter. That is, frequencies less than a cutoff value f_c given by

$$f_c = 1/\pi (LC)^{\frac{1}{2}} = 1/\ell\pi (L'C')^{\frac{1}{2}} \qquad (22)$$

are transmitted, while higher frequencies are totally attenuated. Good frequency response is obtained only up to about half the cutoff value, which implies that the length of the segment must be less than about 1/4 the wavelength of the highest frequency wave for which good response is required, if the lumped-parameter approach is to be a good approximation to the real, distributed-parameter system . This, of course, determines the degree of lumping possible in the model, i.e., the number of segments needed to model a vessel of a given total length.

In the circuit of Figure 7, there is a delay time between the input and output signals consistent with a traveling-wave velocity of, in the lossless (inviscid) case,

$$c = (L'C')^{-\frac{1}{2}} \qquad (23)$$

If the input impedance of the downstream networks does not match the characteristic impedance of a given segment Z_0, given by

$$Z_0 = (R + j\omega L/j\omega C)^{\frac{1}{2}} \qquad (24)$$

then part of the energy will be reflected. Thus, in the general case, waveforms in the system consist of superpositions of both incident and reflected traveling waves.

This type of lumped-parameter approach is practical for the description of blood flow through entire vascular beds. In a formal manner, the L-R-C networks representing each vessel could be connected together in the correct anatomical arrangement to synthesize a complete model for the bed. This, of course, would result in a very large model because vascular beds contain millions of small vessels; however, the networks for entire groups of smaller vessels can be further combined, using the standard rules for series and parallel combinations of electrical elements, into equivalent, more highly lumped L-R-C networks. In this manner, a vascular bed model of a useful size can be developed.

The assumptions upon which the above analysis is based apply best to flow in the arteries. Somewhat different dynamical effects occur in the capillaries[15, 16] and veins[11], but even here the basic forces involved are inertial, viscous, and elastic. It has been found that the flow through the lung capillaries is dominated by viscous (resistive) effects, although the usual Poiseuille resistance law, Equation (14), does not apply[16]; in the veins, the L-R-C circuit as described above provides a good approximation for the flow dynamics[11], although corrections involving variations of the circuit parameters with transmural pressure can be made to account for venous collapse[58].

The inertance, resistance, and compliance in the lumped-parameter model depend on the physical and geometrical properties

of the vascular system. If these properties are known, the parameter values can be calculated using expressions of the type given in Equations (13) to (15). Alternately, the parameters can be calculated by analysis of physiologically measured pressure and flow rate data.

The lumped-parameter approach has been used successfully to develop models of the systemic arterial tree[56] as well as the entire circulatory system[58]. Some work on the pulmonary circulation has also been performed[59-61], but, as will be discussed in more detail in the following section, these previous models had a different purpose than the present model and hence differ from it in several ways.

B. The Mathematical Model and Its Solution

The mathematical model of the pulmonary circulation used in the present study is based on the lumped-parameter description of blood flow in vessels described in the previous section. The model consists of a number of inertance-viscous resistance-compliance networks arranged in a manner consistent with the anatomy of the pulmonary circulation; the equivalent electrical representation of the model in terms of inductance-electrical resistance-capacitance filter circuits is shown in Figure 8. Individual filter circuits are provided for the main pulmonary artery, the left and right pulmonary arteries, and the arteries, precapillaries-arterioles, capillaries, venules, and veins in each of four parallel paths representing the upper and lower lobes in each lung (the middle lobe of the right lung is considered to be part of the lower lobe). The flow paths originate at a point (0) in the main pulmonary artery just downstream from the pulmonary valve and terminate at a point (7) representing the left atrium. The external or perivascular pressures are taken to be intra-thoracic pressure (G_0) for the main, left, and right pulmonary arteries and alveolar pressure (G_1) for the vessels within the lobes of the lungs. The hydrostatic pressures in each lobe of the lungs are represented by voltage (pressure) sources ($G_{11},\ldots,G_{22}$). All pressures are relative to the atmospheric value.

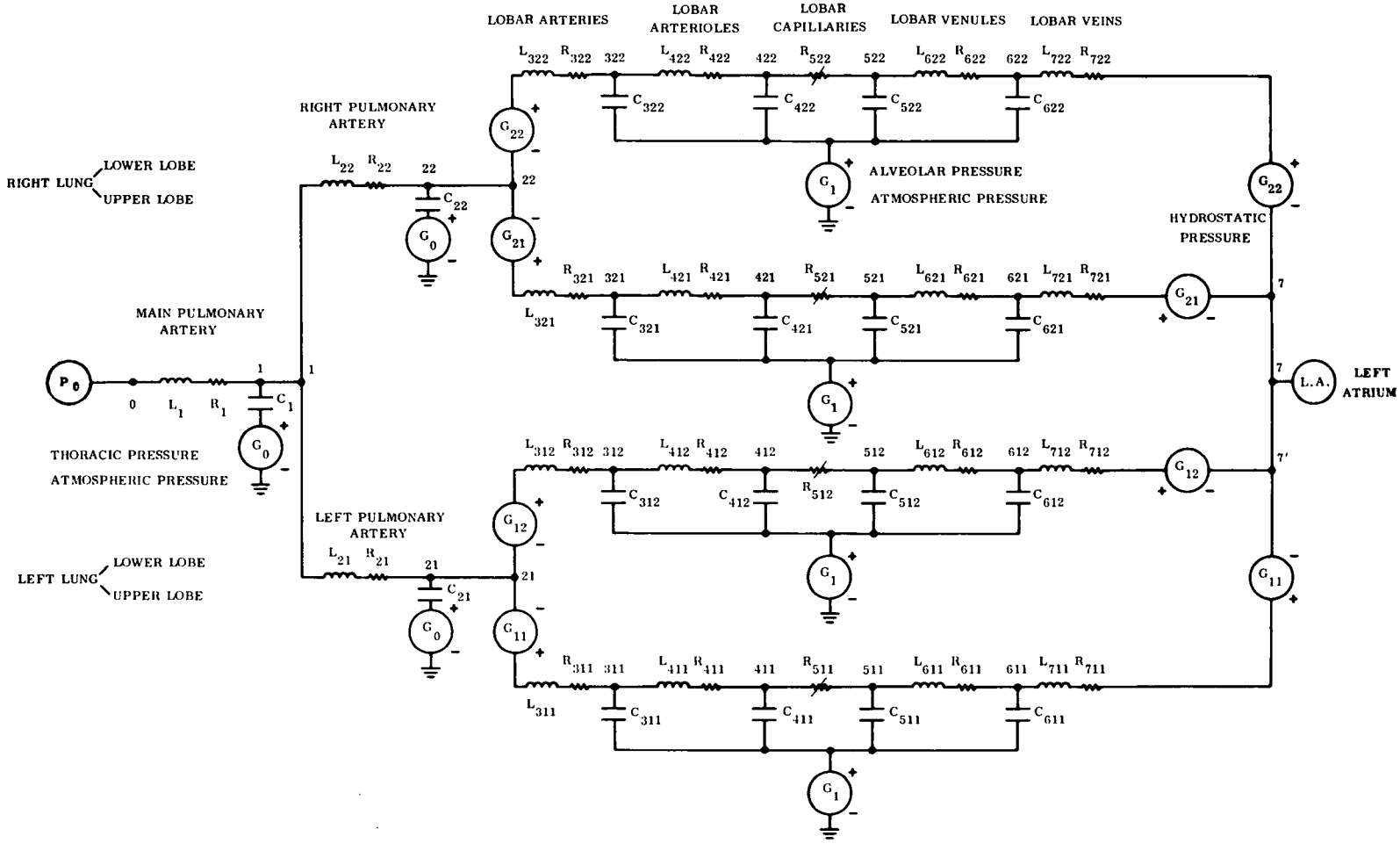

FIGURE 8. THE PULMONARY CIRCULATION MODEL IN ELECTRICAL ANALOG FORM.

The time-dependent pressures at the two ends of the flow path (P_0 and P_7) are considered to be inputs to the model. Their forms, based on physiological data[26,43] with a one-second heart beat period, are shown in Figure 5 (b), as produced by an electronic function generator. Intrathoracic and alveolar pressures as functions of time are also inputs to the model; these pressures are approximated by sinusoids having periods of four seconds, an average respiratory cycle, Figure 6 (b). Similarly, the hydrostatic pressures in each lobe are model inputs; these are constants which depend on the strength and orientation of the applied inertial field.

As discussed in Chapter II the pulmonary circulation is non-linear, the resistance to flow depending strongly on the mean transmural pressure. This makes models having constant properties inaccurate when deviations away from the normal operating point (as occur in abnormal environments or pathological situations) exist. Thus, the present model incorporates the variation of total resistance with mean transmural pressure (but not with instantaneous transmural pressure). The characteristic curve, based on physiological data[22], is shown in Figure 9.

In the implementation of this non-linearity, it is assumed that all of the resistance variations occur in the microcirculation (elements $R_{511},\ldots,R_{522}$ in Figure 8); all other resistances are constant. Thus, the microcirculatory resistances (which are high resistance elements, containing over 80% of the total resistance in each lobe) are allowed to vary with mean transmural pressure in such a way that the total resistance of the system follows the characteristic curve of Figure 9.

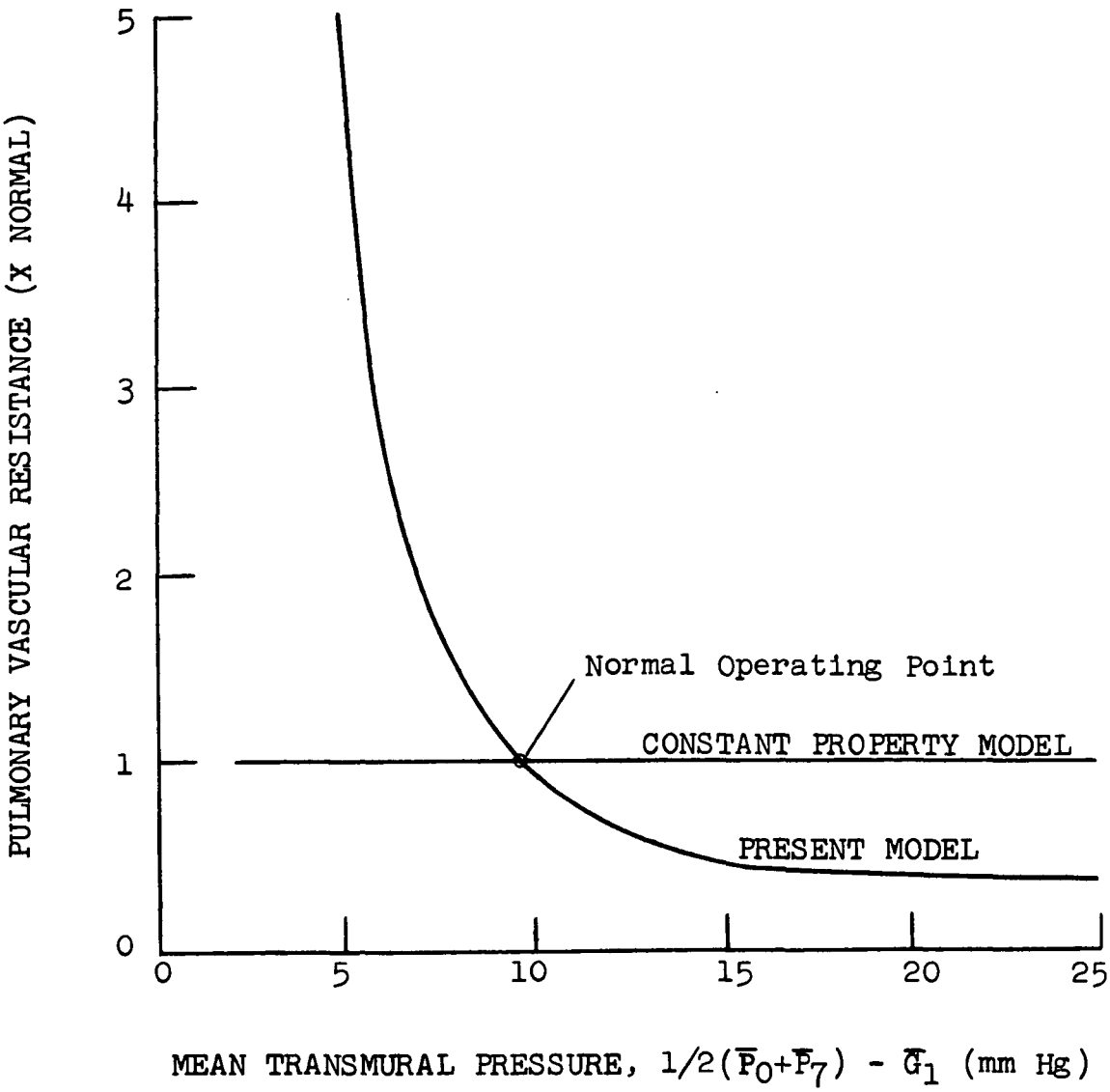

FIGURE 9. VARIATION OF TOTAL PULMONARY VASCULAR RESISTANCE WITH TRANSMURAL PRESSURE.

The inertance and compliance of the pulmonary circulation must also depend on the transmural pressure. However, no physiological data on such variations have been found, and these parameters are assumed to be constant in the present model.

In order to provide a baseline for the simulations, a control state is defined, which consists of a normal subject at rest in the supine position. The parameter values used for this control state are given in Figure 10. Control state resistance values were determined by first noting that the total resistance of the pulmonary circulation is 0.112 mmHg/(cm^3/sec) or 150 dyn sec/cm^5 (fluid ohms), based upon a mean driving pressure (main pulmonary arterial pressure minus left atrial pressure) of 8.4 mm Hg and a mean pulmonary blood flow rate of 75 cm^3/sec or 4.5 l/min. The right lung receives about 55% of the total flow[26], and it was assumed from volume considerations that the lower lobes receive 60% of the flow to each lung. Within each lobe, the resistance was distributed among arteries, precapillaries-arterioles, capillaries, venules, and veins in the ratios 2/4/48/4/1, as suggested by Rideout and Katra[61]. Based on this information, the resistance values were calculated using the usual rules regarding series and parallel combinations of resistances.

Rideout and Katra indicate that the net inductance and capacitance are about 3 dyn sec^2/cm^5 (fluid henrys) and 8.75×10^{-3} cm^5/dyn (fluid farads). Their values of 1 henry and 750 microfarads for the main pulmonary artery were used, and it was assumed that the left and right pulmonary arteries had values of 1 henry and 250

RESISTANCES

dyn sec/cm^5 or fluid ohms	
R_1	2.5
R_{21}, R_{22}	5
R_{311}	28
R_{312}	18.7
R_{321}	23
R_{322}	15.3
R_{411}	56
R_{412}	37.4
R_{421}	46
R_{422}	30.6
R_{511}	670
R_{512}	448
R_{521}	550
R_{522}	366
R_{611}	56
R_{612}	37.4
R_{621}	46
R_{622}	30.6
R_{711}	14
R_{712}	9.4
R_{721}	11.5
R_{722}	7.6

INDUCTANCES

dyn sec^2/cm^5 or fluid henrys	
L_1, L_{21}, L_{22}	1.0
L_{311}, ..., L_{722}	1.5

CAPACITANCES

10^{-6} cm^5/dyn or 10^{-6} fluid farads	
C_1	750
C_{21}, C_{22}	250
C_{311}, ..., C_{322}	125
C_{411}, ..., C_{422}	1250
C_{511}, ..., C_{522}	250
C_{611}, ..., C_{622}	250

PRESSURES

(GENERATED FUNCTIONS)

mmHg	
$\overline{P}_0$	13.4
$\overline{P}_7$	5.0
$\overline{G}_0$	-5.5
$\overline{G}_1$	0
G_{11}, ..., G_{22}	0

FIGURE 10. PARAMETER VALUES FOR THE SIMULATION OF THE CONTROL STATE.

microfarads each. It was further assumed that the remaining inductance and capacitance was equally distributed among the four lobes, with distributions among arteries, arterioles, capillaries, venules, and veins within each lobe given by the ratios 1/1/1/1 for inductance and 1/10/2/2 for capacitance[61]. Again, the rules for series and parallel combinations of circuit elements were used in these parameter determinations.

With these parameter values, the cutoff frequency of the model segment representing the main pulmonary artery is about 12 hz, based on Equation (22). Good response is to be expected to about half this value, i.e., 6 hz or the first six harmonics of the waveforms. In the pulmonary circulation frequencies of up to 10 hz are of interest in studies of the details of wave propagation and reflection[60]. However, the amplitudes of the higher harmonics are relatively low, so that the frequency response of the present model is adequate for the model's purpose, which is the simulation of the characteristic changes in mean values and shapes of the pressure and flow rate waveforms brought about by abnormal environments and pathological conditions. If a higher frequency response was required, this could be achieved by adding more segments to the arterial end of the model.

One of the salient characteristics of the circulatory system is the ability of the heart to adjust the blood pressure levels it produces in response to changes in system parameters, the purpose being to maintain a blood flow rate consistent with the body's metabolic needs. In order that the present model might adequately

simulate the behavior of the real system over wide ranges of the system parameters, a control system (Figure 11) is introduced to account for the adjustment of mean pulmonary arterial pressure. The controlled variable is the mean pulmonary blood flow rate, which is made to match a set point value $\overline{Q}_I^*$ (e.g., normal cardiac output) to within some allowable error ϵ by adjusting the level of the mean pulmonary arterial pressure $\overline{P}_0$, which is an input function. Adjustments of $\overline{P}_0$ also change the mean transmural pressure, and thus also require adjustment of the microcirculatory resistances $R_{511}, \ldots, R_{522}$, in accordance with the pulmonary circulation's resistance characteristic (Figure 9). Because of this nonlinearity, the implementation of this control loop generally requires an iterative procedure.

The computation of the time-dependent pressure at each node and the flow rate through each resistance in the model requires the solution of equations of the type given in Equations (20). In the model, 19 pressures and 23 flow rates must be calculated. The pressure and flow rate equations for each model segment are coupled, both to each other and to those describing the model segments upstream and downstream. Thus, solution of the model requires the simultaneous integration of a large number of coupled equations. This is accomplished on a real-time basis by the use of a general purpose hybrid computer (Astrodata-Comcor 550) located in the General Electric Company's Hybrid Simulation Laboratory. The solution technique largely uses the electronic analog capability of the machine. A basic analog computer circuit

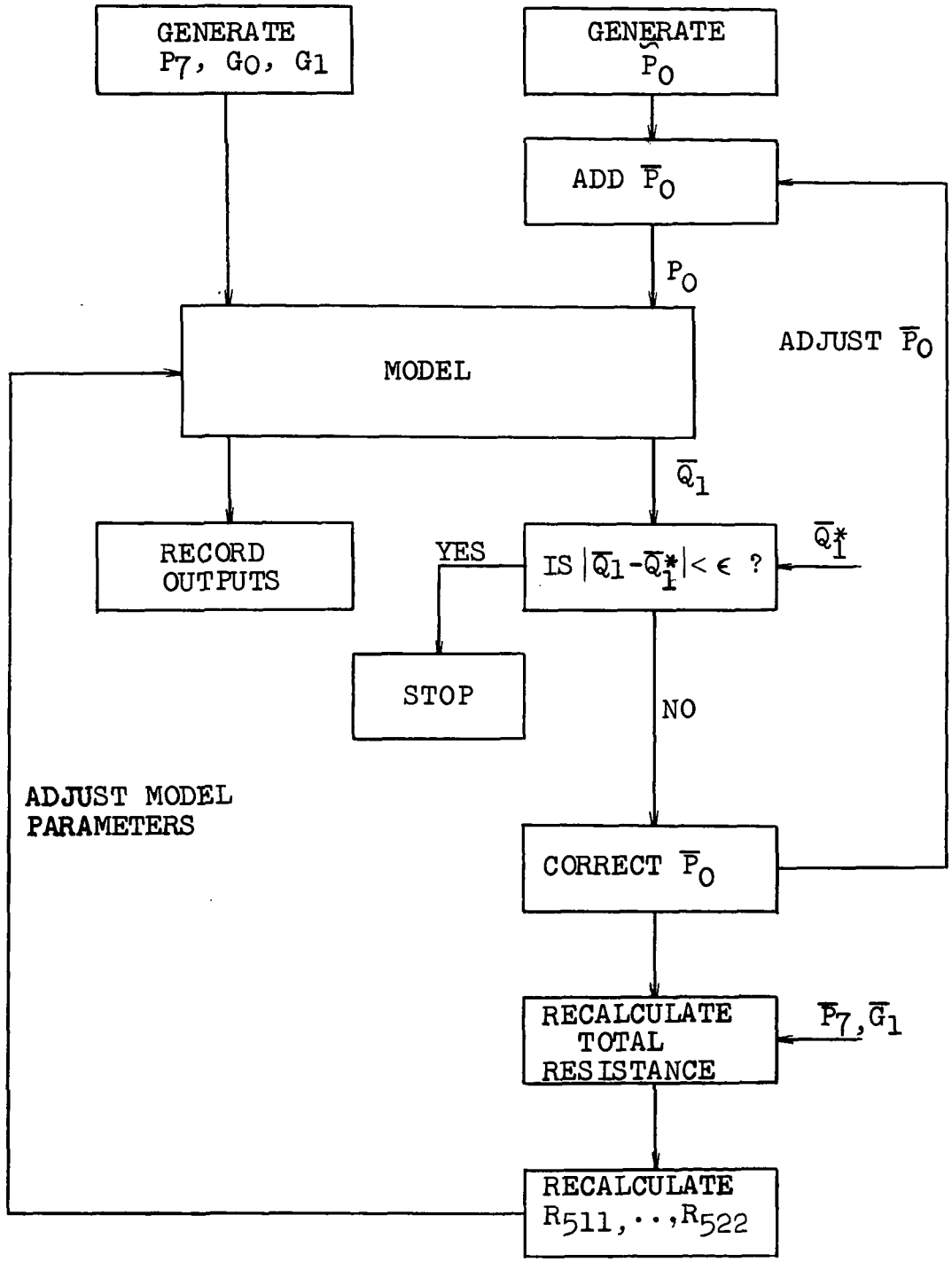

FIGURE 11. FLOW CHART FOR THE CONTROL OF MEAN PULMONARY BLOOD FLOW RATE BY ADJUSTMENT OF MEAN PULMONARY ARTERIAL PRESSURE.

for one vascular segment of the model is shown in Figure 12 and consists of two integrators, one summer, and four coefficient potentiometers. The inlet pressure P_i and outlet flow rate Q_o are input functions in this circuit, with P_i coming from the upstream circuit and Q_o as feedback from the downstream circuit. Minor variations of this basic analog circuit occur in the system. An important feature of the computation scheme is that the settings of the coefficient potentiometers (i.e., the system parameters) can be easily changed by the computer operator; thus, simulations of a wide variety of environmental and pathological situations, each of which manifests itself by some combination of changes in the system parameters or input functions, can be readily performed.

Three 8-channel high-performance pen recorders (Brush Mark 200; frequency response to 55 hz) are used to plot the computed time-varying pressures, flow rates, and volumes. Thus, 24 simultaneous outputs can be displayed.

In performing simulations of the effects of abnormal environments or pathological conditions, the parameter changes which characterize each situation are first determined from data in the published physiological and medical literature. As examples, gravitational fields cause hydrostatic pressures, G_{ij}; vascular deconditioning causes increases in system compliances; embolism in the left lower lobar arteries causes an increase in R_{312}; mitral stenosis causes an increase in P_7, and so on. These parameter changes are

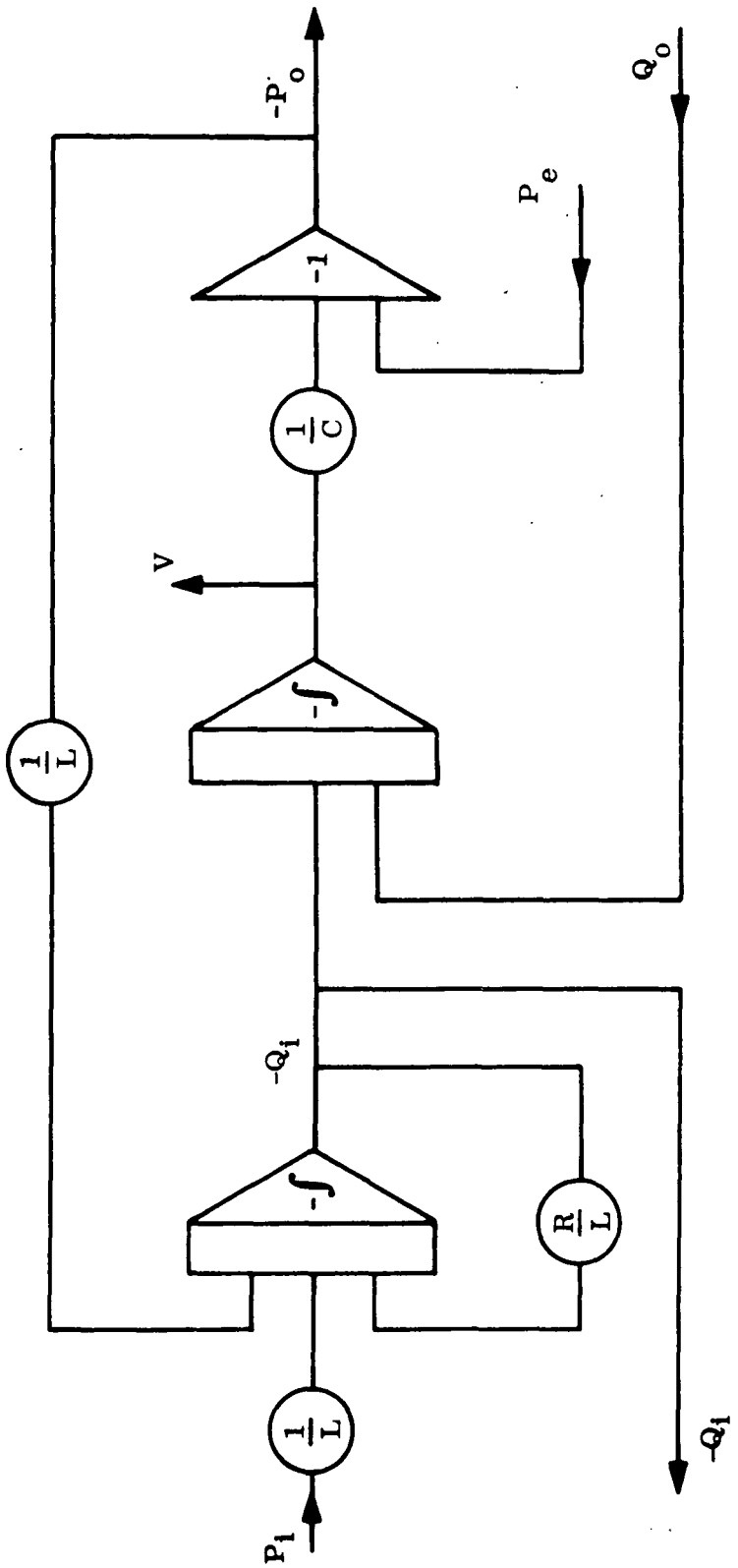

FIGURE 12. ANALOG COMPUTER CIRCUIT FOR A VASCULAR SEGMENT.

introduced into the computer and the calculation initiated. If the total blood flow rate calculated does not agree with the set point value, the control loop (Figure 11) is used to adjust the mean pulmonary arterial pressures and microcirculatory resistances, and the calculation is repeated iteratively until agreement is reached. Although the control loop can be automated, it has been found that agreement on flow rate to within 5 cm^3/sec can usually be achieved within two or three iterations even when the implementation is by hand.

Several other models of pulmonary blood flow have appeared in the literature. Wiener et al.[59] used a digital simulation, based on the flow impedance concept, to study wave propagation through the pulmonary circulation. An analog simulation for investigating input impedance, wave travel, and wave reflection has been described by Pollack et al.[60]; however, the model is confined to the largest arteries, with small arteries, capillaries, and the entire venous side of the circulation represented only by series resistance. The model of Rideout and Katra[61] also uses an analog simulation to simulate the waveshapes of the pressures and flows, and in many respects is similar to the present model.

These previous models all have constant properties and hence do not include the important variation of flow resistance with transmural pressure. Also, they do not include the control loop which adjusts arterial pressure to meet the required level of blood flow rate. None has included environmental parameters such as

hydrostatic pressure heads, and none has been used in a systematic way to study the effects of parameter changes on pulmonary circulation dynamics and to simulate conditions of interest in environmental physiology and medicine, which are the goals of the present work. On the other hand, the previous models have better frequency responses than the present model. In general, the differences among the various models, including the present one, are consistent with their individual purposes.

IV. SIMULATIONS OF PULMONARY CIRCULATORY DYNAMICS

A. The Range of Environmental and Pathological Conditions Simulated

The mathematical model described in the previous chapter has been applied to the investigation of the effects of abnormal environments and pathological conditions on the pulmonary circulation. Twenty different conditions were simulated. The first of these is a control or baseline case with which the others can be compared:

1. Control (normal subject at rest in the supine position).

Eight of the simulations treat the effects of abnormal environments. These include:

2. Zero G_Z (effect of weightlessness on a normal pulmonary vascular bed)
3. Zero G_Z with vascular deconditioning (effect of weightlessness on a vascular bed having increased compliance due to adaptation to the weightless environment)
4. One G_Z (effect of terrestrial gravitational force, acting along the body axis, on a normal pulmonary vascular bed)
5. One G_Z with vascular deconditioning (effect of terrestrial gravitational force on a pulmonary vascular bed which has been adapted to a weightless environment)
6. Three G_Z (effect of a hypergravic environment on a normal lung)

7. Increased alveolar pressure (effect of increased external pressure on the vascular bed, due to an artificial breathing system)
8. Exercise (effect of increased cardiac output in a normal lung)
9. Hypoxia (effect of arteriolar spasm or vasoconstriction due to low alveolar oxygen pressure).

Eleven pathological conditions were simulated, including:

10. Local pulmonary embolism (effect of multiple emboli occluding the small arterial branches in one lobe of one lung)
11. Diffuse pulmonary embolism - 50% occlusion (effect of occlusion of half the microcirculatory vessels throughout the lungs)
12. Diffuse pulmonary embolism - 75% occlusion (effect of occlusion of 3/4 of the microcirculatory vessels throughout the lungs)
13. Excision of right lung (effect of surgical removal of half the total pulmonary vascular bed)
14. Circulatory shock (effect of decreased cardiac output)
15. Mitral stenosis (effect of increased left atrial pressure)
16. Atrial septal defect with normal vascular properties (effect of increased blood flow rate)

17. Atrial septal defect with reactive vascular changes (effect of increased blood flow rate when vascular fibrosis has occurred)
18. Emphysema (effects of obliteration of part of vascular bed plus vasoconstriction due to hypoxia)
19. Interstitial fibrosis under rest conditions (effect of decreased vascular compliance when cardiac output is normal)
20. Interstitial fibrosis during exercise (effect of decreased vascular compliance when cardiac output is increased).

These particular conditions were chosen for simulation because of their importance in present-day environmental physiology and clinical medicine and because, in most cases, physiological data for comparison with the model predictions exist in the literature. In addition, these simulations encompass a wide variety of situations which may occur in the pulmonary circulation, including cases in which the blood flow rate is increased (8,9, 16-18,20) and decreased (6,14) from normal; main pulmonary arterial pressure is elevated (8-13, 15-18, 20) and reduced (14) from normal; left atrial pressure is elevated (15) and reduced (14); alveolar pressure is elevated (7); the hydrostatic pressure heads are varied (2-6); and the vascular resistance (4-18, 20) and compliance (3, 5, 9-13, 17-20) deviate from their normal values.

Examples of pulmonary hypertension due to obstructive (10-12), vasoconstrictive (9, 18), obliterative (13, 18), hyperkinetic (16, 17), and passive (15) mechanisms have been included.

B. Results of the Simulations

Control State - The control state has been defined as that existing for a normal, healthy subject at rest in the supine position. In this state, the hydrostatic heads in the model are zero; that is, gravitational loadings have no effect on the model. To simulate the control state, all of the system parameters and input functions were set at their control values (Figure 10), and the pulmonary blood flow rate set point $\bar{Q}_1^*$ was made equal to the normal cardiac output, assumed to be 4.5 l/min. The time-dependent pressures and blood flow rates throughout the system were then computed and recorded. The computer outputs are shown in Figures 13 and 14; a four-second time interval is illustrated so that the depicted results cover an entire respiratory cycle, the longest repetitive period in the model.

The computations indicate that the pressure waveforms are continuously changed as they pass through the vascular bed (Figure 13). On the arterial side, mean pressure drops only by about 1 mm Hg between the main pulmonary artery and the lobar arterioles; the pulse pressure (maximum minus minimum pressures during one pulse cycle), however, decreases from 10 mm Hg in the main pulmonary artery to about 7.5 mm Hg in the arterioles due to damping of the pulsation by the vascular compliance. This damping also progressively decreases the amplitude of the secondary (diastolic) peak in the arterial pressure pulse and causes a general smoothing of the waveform. It should be noted that the "peaking" of the pressure pulse as it travels through the arterial side of the bed is not

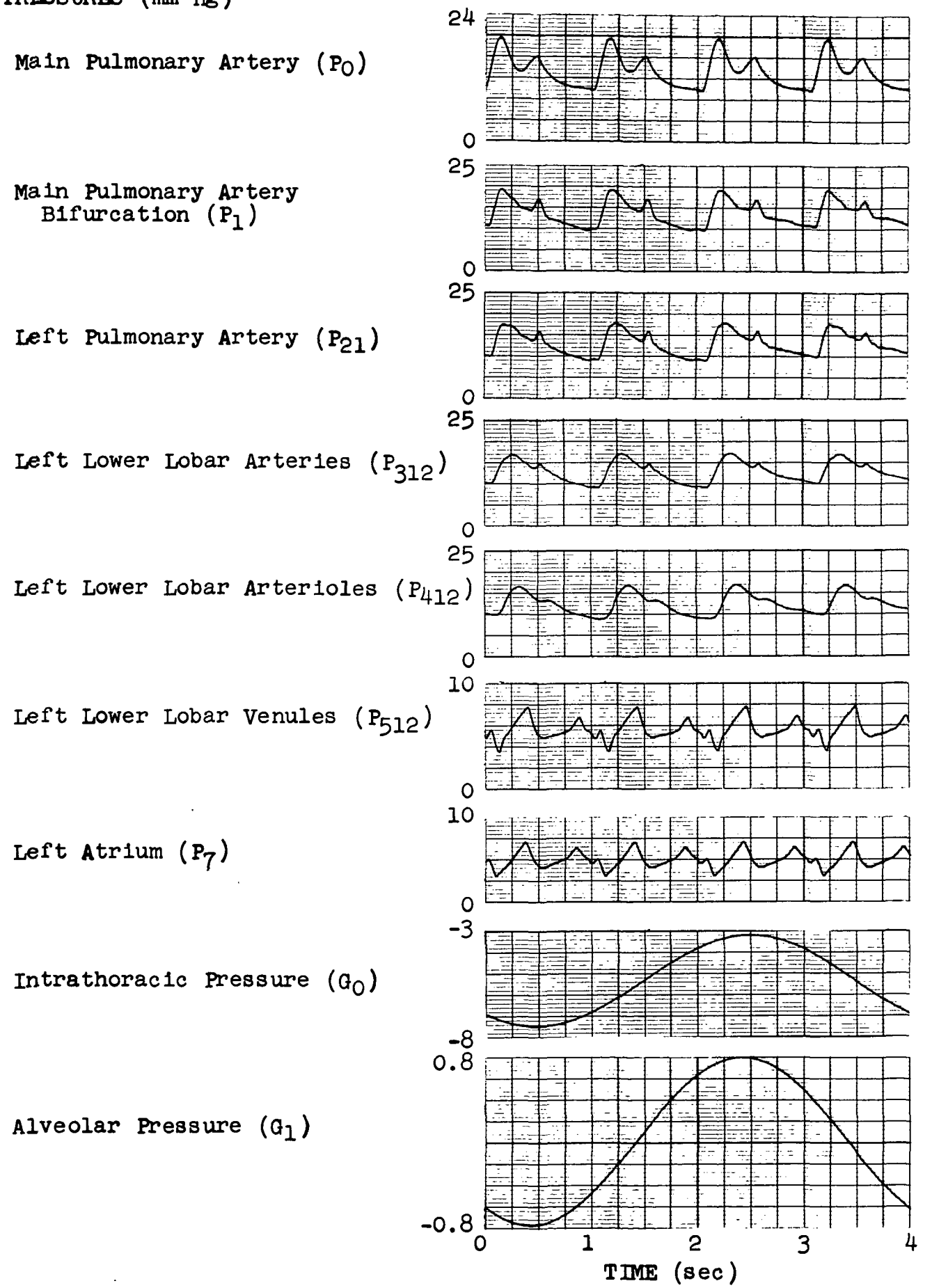

FIGURE 13. SIMULATION OF THE CONTROL STATE - PRESSURES.

observed in the present results, although other models[59,60] have indicated such a result; this phenomenon has been observed experimentally in the systemic circulation, but its existence in the pulmonary circulation has apparently not been firmly established.

Most of the pressure drop in the model occurs between the arterioles and venules, i.e., in the microcirculation, and this pressure difference is computed to be about 7 mm Hg. Mean capillary pressure is about 9 mm Hg, which is close to the value of 10 mm Hg estimated by Fishman[26].

Pressure in the venules is quite pulsatile and rather closely follows events in the left atrium, although some differences in waveshape exist. The computed mean pressure in the venules was about 5.5 mm Hg, which agrees very well with experimental data[62] if it is assumed that arterial wedge pressure measurements approximate the pressure in the venules; the computed venule pressure waveshape also compares well with pulmonary arterial wedge tracings[28]. The pressure drop between the venules and left atrium is only about 0.5 mm Hg, indicative of the low resistance of the pulmonary veins.

The computed flow rate through the main pulmonary artery (Figure 14) has a strong pulsatile nature; it is zero over that portion of the pulse cycle when the pulmonary valve is closed. This behavior closely approximates the experimental evidence[59].

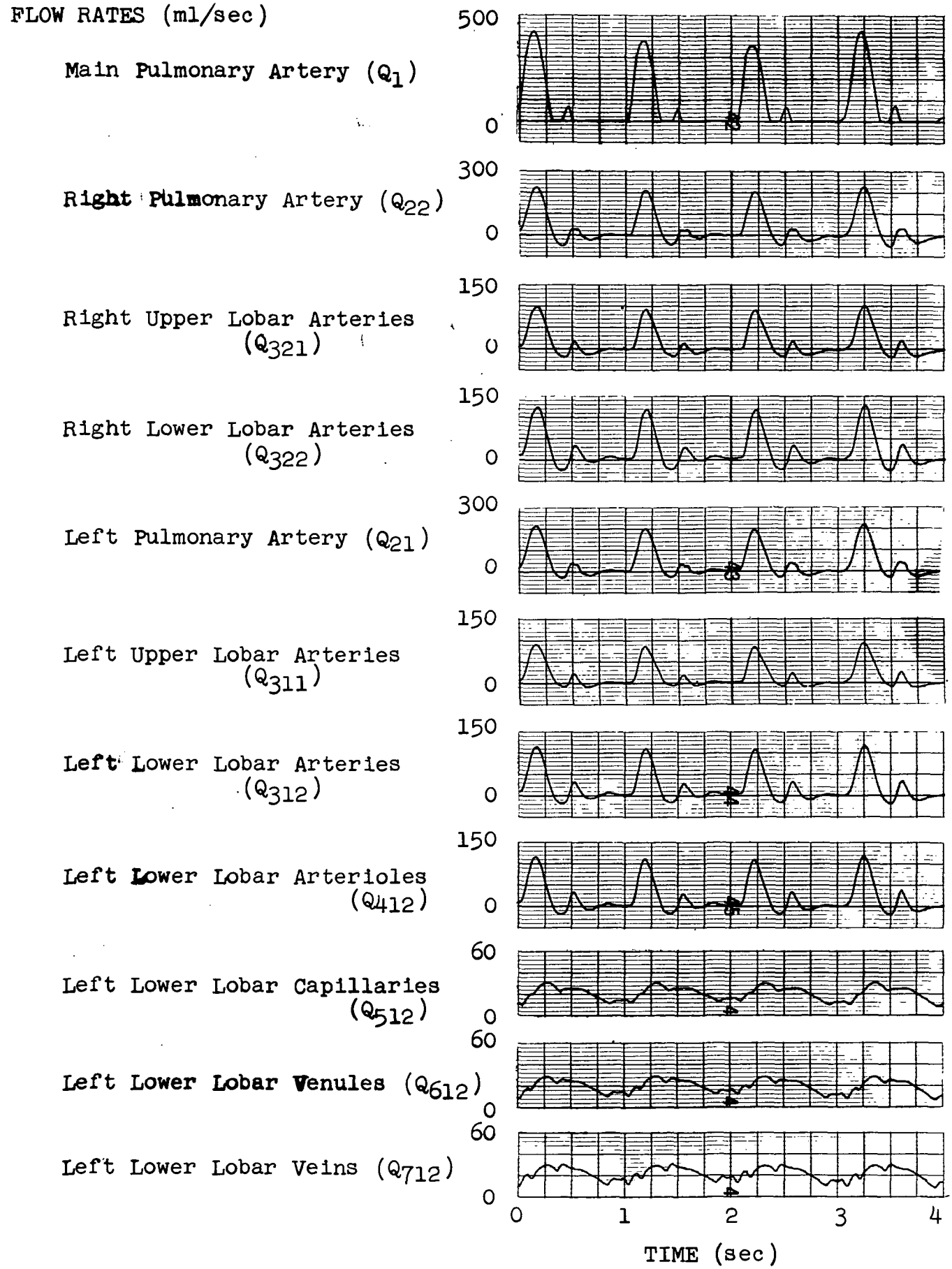

FIGURE 14. SIMULATION OF THE CONTROL STATE - FLOW RATES.

Blood flow rates through the left and right pulmonary arteries, lobar arteries, and lobar arterioles are all highly pulsatile and, in general, similar in form to one another. There appears to be relatively little damping of the flow pulse through these vessels. All of these computed flow pulses show two brief periods of backflow during diastole. It should also be noted that the flow rates through the various lobes differ from one another because each lobe in the model has individual properties.

In the capillaries, the computed flow rate is still unsteady, but the pulsations have been strongly damped so that no backflow occurs; the amplitude of the oscillatory component of the waveform is only about half the mean value. This unsteady behavior of the pulmonary capillary blood flow has been well established experimentally[26].

The computed flow rate in the lobar veins is also unsteady and contains five distinct maxima per pulse cycle. The waveshapes yielded by the model are consistent with physiological measurements made by Kennen et al.[63], who also explained the presence of the five maxima per pulse in terms of events in both the right and left hearts.

The pressure and flow waveforms yielded by the model show successive time displacements indicative of traveling-wave propagation of the pressure and flow pulses. In the large arteries, the results yield a propagation speed of between 200 and 300 cm/sec

for the pressure pulse, which is consistent with physiologically measured values[26,60]. On the venous side, there is also a time delay between events in the left atrium and those in the venules; this indicates the propagation of a retrograde wave from the left atrium back into the pulmonary circulation with a propagation speed of about 300 cm/sec. Such retrograde waves have been noted previously[59], and the computed propagation speed compares well with data in the physiological literature[28].

The effects of the respiratory cycle on events in the pulmonary circulation are easily seen in the computed results. On the arterial side, the diastolic pressures are highest during expiration, as are the peak blood flow rates. These effects are less pronounced on the venous side. Although the behavior predicted by the model is approximately in agreement with physiological data[26,28,34,59] there are some discrepancies (e.g., the model does not predict the observed rise in systolic pressure during expiration); the relationships between respiration and the pulmonary circulation are complex and not fully understood, and it is quite possible that the model is incomplete in this aspect of pulmonary circulatory dynamics.

Pulmonary arterial pressure, left atrial pressure, alveolar pressure, and pulmonary blood flow rate are dominant variables in the pulmonary circulation. In order to determine their influence on this vascular bed, a series of "experiments" was performed on the model; in each of these "experiments", two of the four important

variables were held fixed, and the quantitative relationship between the other two was determined. In these "experiments", system parameters other than the variable capillary resistances were held at their control values.

In the first "experiment", the pulmonary blood flow rate set point $\bar{Q}_1^*$ was varied from 0 to 20 l/min, and the influence of this flow rate on the pulmonary arterial pressure P_0 was calculated; left atrial and perivascular pressures were held fixed. It was found that the arterial pressure-flow rate relationship is non-linear (Figure 15), in consequence of the variability of vascular resistance with transmural pressure. When the flow rate is low, the arterial pressure required to drive the flow is also low, which causes a relatively low transmural pressure and relatively high resistance. As flow rate increases, the required arterial pressure rises, causing an increase in transmural pressure and decrease in resistance. When the flow rate is about three times normal, the transmural pressure is high enough so that expansion or recruitment in the vascular bed is complete; thereafter, the arterial pressure-flow rate relationship becomes linear. This computed behavior follows the measured behavior very well[22,26], since the resistance relationship used in the model is based on physiological data derived from arterial pressure and flow rate measurements. In Figure 15, it is seen that the arterial pressure-flow rate relationship predicted by a constant-property model does not yield realistic results if the system is operating away from

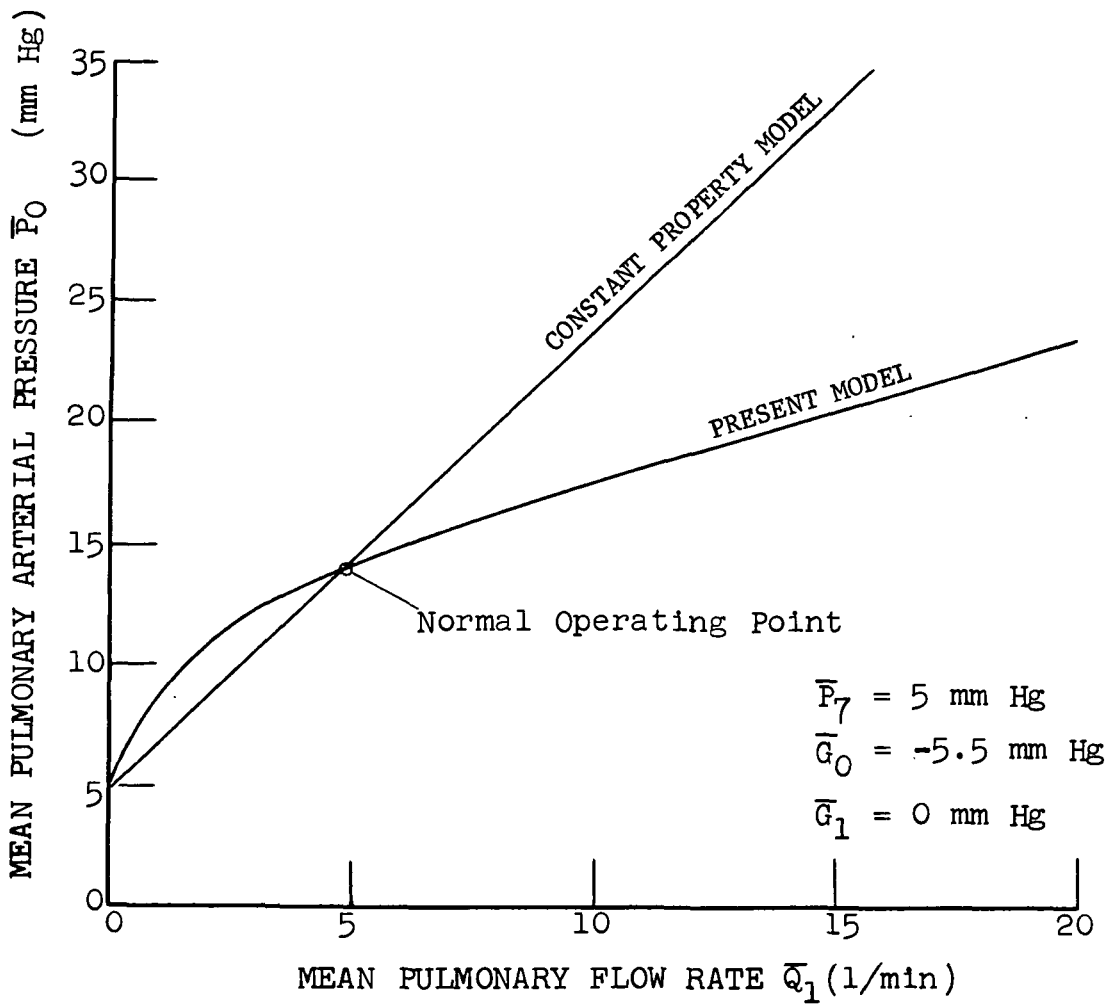

FIGURE 15. EFFECT OF PULMONARY BLOOD FLOW RATE ON PRESSURE IN THE MAIN PULMONARY ARTERY.

its normal operating point; thus, such a model would yield poor simulations of the effects of exercise or hyperkinetic disease, in which flow rate may be many times normal.

In a second "experiment", the mean left atrial pressure was varied from 0 to 30 mm Hg, and its influence on the pulmonary arterial pressure P_O was determined; pulmonary blood flow rate and perivascular pressures were held fixed. The results, shown in Figure 16, indicate that the relationship between pulmonary arterial pressure and left atrial pressure is highly non-linear. Pulmonary arterial pressure is almost constant when left atrial pressure is in the range from 0 to about 10 mm Hg (i.e., about 5 mm Hg on either side of its normal value). However, when left atrial pressure rises higher than about 10 mm Hg, pulmonary arterial pressure must rise in compensation in order that the same flow rate be maintained. This non-linear behavior is a consequence of the variation of vascular resistance with transmural pressure. Its significance is that, over a limited range, the right heart can operate at an approximately constant load, despite changes in the left heart. It should be noted that the relationship predicted by the model agrees very well with physiological data[22,35]; on the other hand, a constant-property model would yield a linear relationship (Figure 16) which is not in agreement with reality. For example, the present, non-linear model predicts that pulmonary edema (exudation of fluid from the capillaries into the alveoli) can occur when the left atrial pressure exceeds about 26 mm Hg, while the constant-property model predicts a value of 23 mm Hg; the values given in the literature are about 27 mm Hg[22,64].

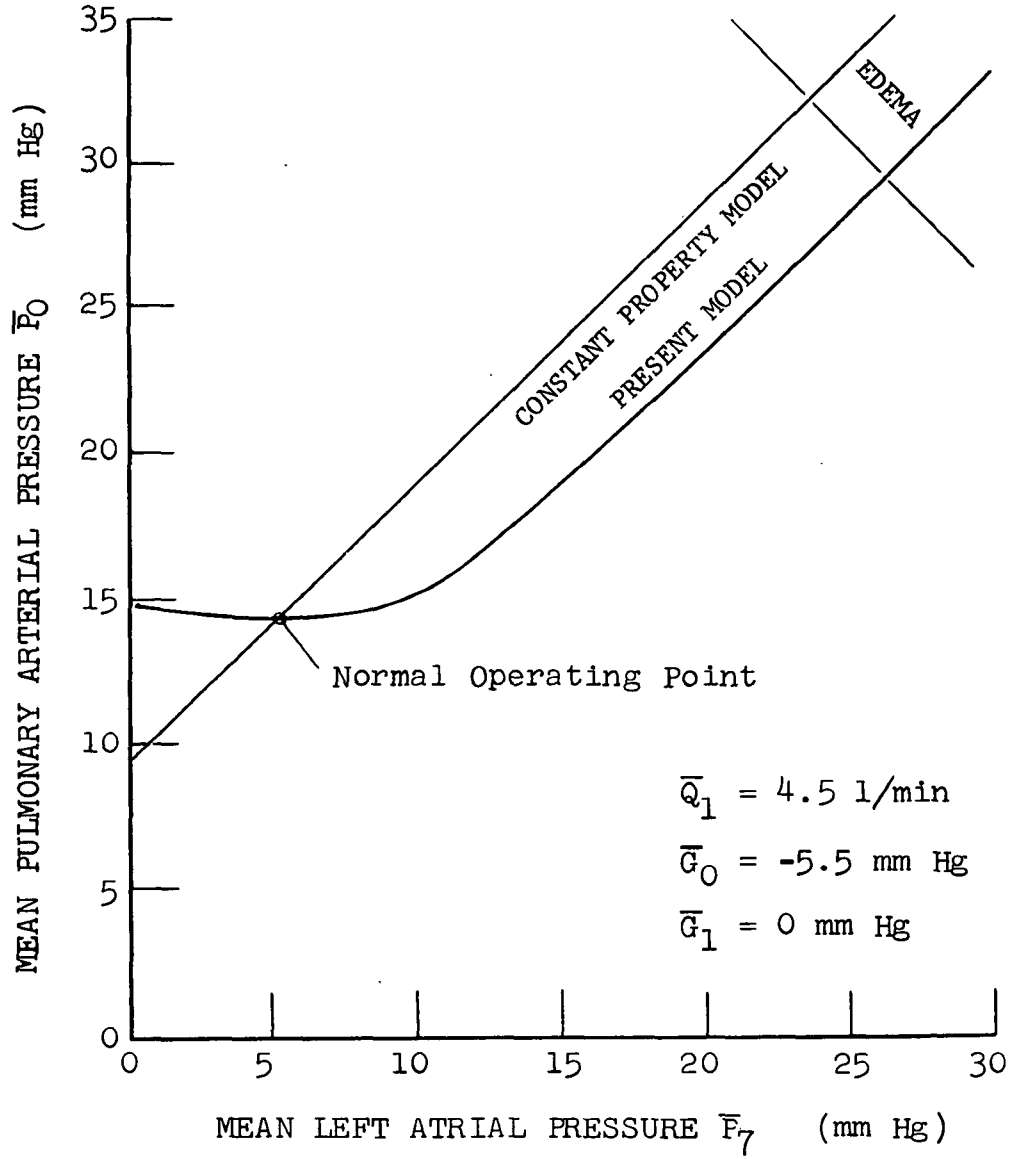

FIGURE 16. EFFECT OF LEFT ATRIAL PRESSURE ON PULMONARY ARTERIAL PRESSURE.

The effect of left atrial (i.e., pulmonary venous) pressure on the blood flow rate through the lungs was investigated in a third "experiment", with pulmonary arterial and alveolar pressures held fixed; in a fourth "experiment", the effect of alveolar pressure on blood flow rate was determined, holding pulmonary arterial and left atrial pressures constant. These two experiments are related and can be discussed together; the computed results are shown in Figures 17 and 18.

In Figure 17, venous pressure was progressively decreased from 20 mm Hg to 5 mm Hg; with arterial pressure held at 20 mm Hg, this corresponds to an increase in the arterio-venous pressure difference (driving pressure) from 0 to 15 mm Hg. As the driving pressure increases from zero, the blood flow rate initially increases proportionally. However, when the venous pressure reaches about 10 mm Hg (i.e., about 5 mm Hg above the alveolar pressure), the blood flow rate reaches a maximum value, and further decreases in venous pressure actually cause a slight decrease in flow rate, despite the fact that the driving pressure continues to increase.

In Figure 18, alveolar pressure was decreased from 20 mm Hg to -15 mm Hg, holding arterial and left atrial (venous) pressures fixed. Thus, the driving pressure was constant at 20 mm Hg, but the arterio-alveolar pressure difference increased from 0 to 35 mm Hg. When alveolar pressure was equal to arterial pressure, the flow rate was zero. Flow began when the alveolar pressure decreased below about 10 mm Hg. As alveolar pressure decreased further, the flow rate increased strongly, until reaching a plateau when alveolar pressure

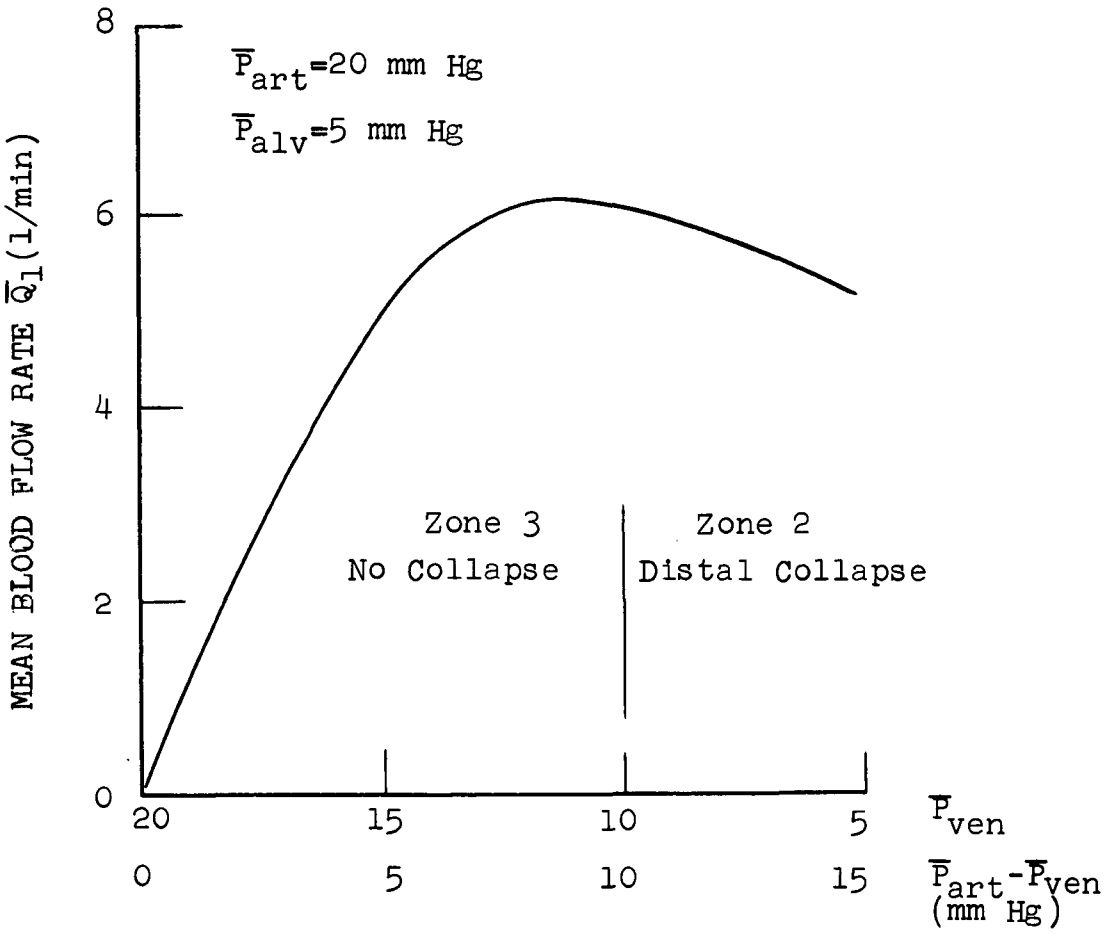

FIGURE 17. MODEL PREDICTION OF THE EFFECT OF VENOUS PRESSURE ON PULMONARY BLOOD FLOW RATE.

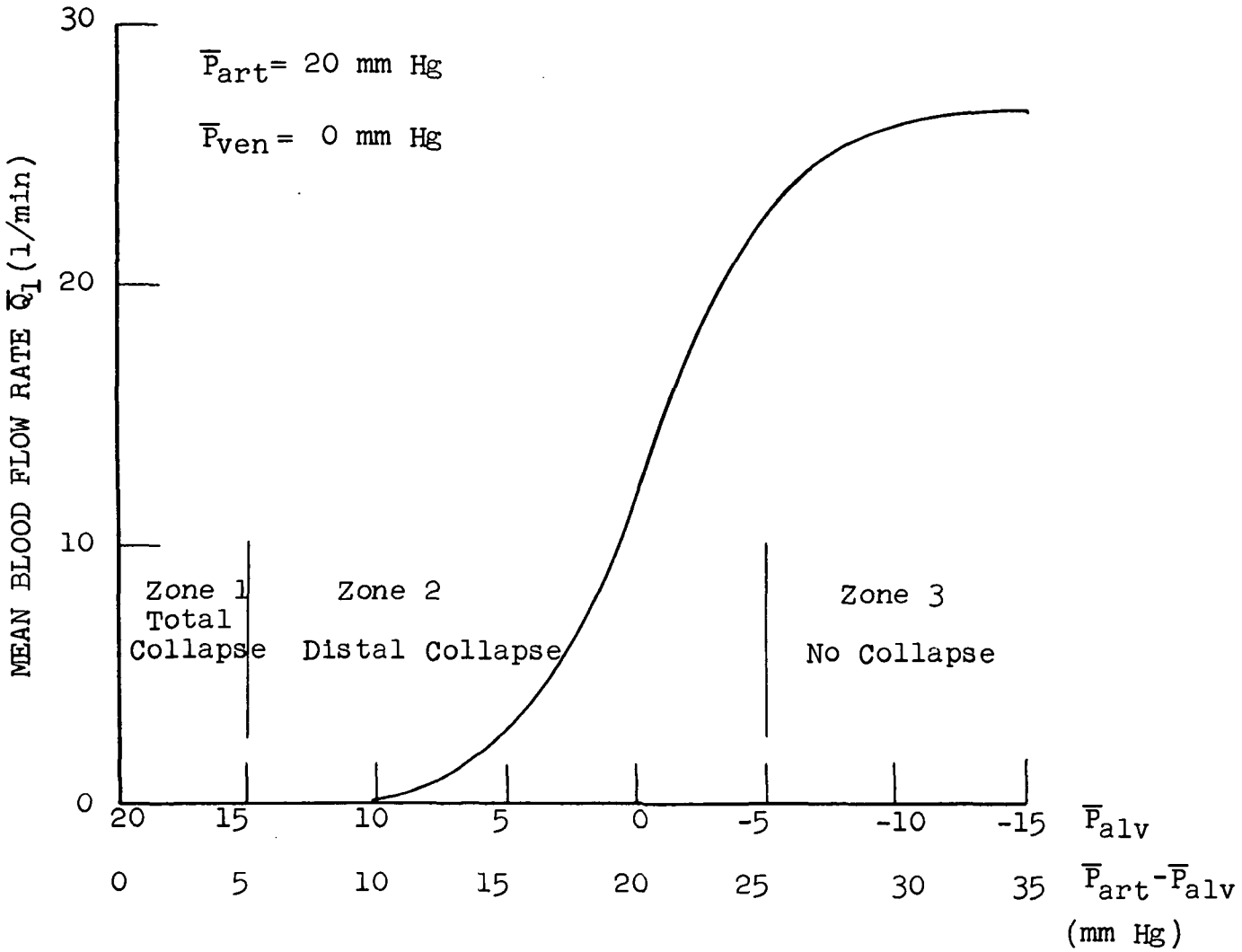

FIGURE 18. MODEL PREDICTION OF THE EFFECT OF ALVEOLAR PRESSURE ON PULMONARY BLOOD FLOW RATE.

reached about -5 mm Hg (i.e., about 5 mm Hg below the venous pressure level).

Many aspects of the non-linear behavior exhibited by the present model have been observed in physiological experiments, e.g.,[32,35,38,40,41]. The behavior can be understood in terms of the variation of vascular resistance with transmural pressure. In the literature, the non-linear behavior of the pulmonary vascular bed has been explained in terms of vessel distensibility by the so-called "sluice hypothesis"[35] or "vascular waterfall hypothesis"[40]; West[46] has categorized the various important regimes as "zones".

According to these explanations, local capillary beds behave as Starling resistors; that is, they dilate or constrict in response to the local levels of arterial, venous, and alveolar pressure. If alveolar pressure is less than both arterial and venous pressures, the bed is open, and the blood flow rate depends on the arterio-venous pressure difference, that is, on the driving pressure (West's Zone 3). If alveolar pressure is intermediate between the arterial and venous pressures there is a partial collapse of the vessels in their distal sections, and under these conditions it has been found that the flow rate depends primarily on the arterio-alveolar pressure difference and is relatively insensitive to the venous pressure (Zone 2). If alveolar pressure exceeds arterial pressure, the bed is completely collapsed, the resistance becomes infinite, and blood flow ceases (Zone 1).

The boundaries separating the various zones are also shown in Figures 17 and 18. These boundaries account for the fact that the resistance in the model becomes infinite when the transmural pressure is less than about 5 mm Hg (see Figure 9), which is then a "critical closing pressure"[32] (in the literature, explanations of the non-linear phenomena in the pulmonary circulation generally ignore any critical closing pressure). It is seen that the model predictions agree very well with the physiological observations: in Zone 1 there is no flow; in Zone 2, the flow rate depends primarily on the arterio-alveolar pressure difference, and is relatively insensitive to venous pressure (the slight decrease of flow rate as venous pressure decreases has been observed in dogs[40]); and in Zone 3, the flow rate depends on the arterio-venous pressure difference, but is insensitive to alveolar pressure. This behavior of the model allows its application to the simulation of the effects of inertial loadings, where the various effects of arterial, venous, and alveolar pressures are very important[46].

Inertial Loadings and Vascular Deconditioning

The hydrostatic pressures in the pulmonary blood vessels due to gravitational forces may be comparable to, or even larger than, the normal blood pressure developed by the right heart. These additional pressures, which vary throughout the lungs, alter the distributions of transmural pressure and vascular resistance and thus change the distribution of perfusion in the lungs. On the other hand,

hydrostatic pressures are absent during weightlessness (zero-G), and in this state the distribution of pulmonary perfusion is quite uniform and probably ideal[48]. Thus, weightlessness is not expected to have a deleterious effect on the pulmonary circulation, but high gravitational fields could possibly alter the blood flow through the lungs enough to cause severe problems.

During long periods of weightlessness, the vascular system may become deconditioned. That is, due to the absence of the stimuli caused by gravitational loadings, the structures within the vessel walls, particularly muscle, may adapt to the new environment by losing some of their tone. This increases the compliance of the bed. Although this would have little effect as long as the body is in the zero-G environment, upon return to a 1-G environment or during atmospheric re-entry (when the inertial loading is several G's) the increased compliance could possibly cause a pooling of the blood in the lungs (and in the large systemic veins, where the effect may be even greater)and other abnormal hemodynamic effects. These phenomena are difficult to study experimentally, so that computer simulations are useful in identifying potential hazards and in guiding experimental research.

Five simulations involving inertial loadings and vascular deconditioning were made; these included zero-G with and without vascular deconditioning; 1-G with and without deconditioning; and 3-G without deconditioning. In all cases, the gravitational force vector was assumed to be aligned in the head-to-foot direction, that is, $G = G_Z$.

The simulation of zero-G without deconditioning is identical to that of the control state. The effects of deconditioning were then added by increasing compliances on the arterial side by between 20% and 60%; the new values were $C_1 = 900 \times 10^{-6}$, $C_{21} = C_{22} = 300 \times 10^{-6}$, $C_{3ij} = 200 \times 10^{-6}$, and $C_{4ij} = 1875 \times 10^{-6}$ fluid farads. Resistances and the blood flow rate set point remained fixed at the control values.

In the simulation of $1\text{-}G_z$, it was assumed that the center-of-gravity of the upper lobes is located 5 cm above, while that of the lower lobes is 1 cm below, the level of the large pulmonary arteries; correspondingly, the hydrostatic pressures G_{11} and G_{21} were adjusted to -3.6 mm Hg, while G_{12} and G_{22} were set at +0.72 mm Hg. The transmural pressures in the lobes are altered by these hydrostatic heads, but not by the full amount of the hydrostatic pressure change in the blood; due to the properties of lung tissue itself, an opposing tissue pressure equal to about 25% to 30% of the blood's hydrostatic pressure is also created[49,50]. Thus, the effective change in transmural pressure is only about 70% of the hydrostatic head in the blood; in the simulation, transmural pressure changes of +0.5 mm Hg in the lower lobes and -2.5 mm Hg in the upper lobes were used. Main pulmonary arterial pressure and left atrial pressure were assumed to remain at their control values, as were all other system parameters except the capillary resistances, which depend on the transmural pressures in each lobe (Figure 9), and the pulmonary blood flow rate, which was allowed to vary in response to the change in overall system resistance.

The effects of vascular deconditioning on the pulmonary circulation in a 1-G environment were simulated by introducing the compliance changes characteristic of the deconditioned state, as given above, as well as the hydrostatic and transmural pressure changes corresponding to the 1-G_z loading.

In the simulation of 3-G_z, the hydrostatic pressures G_{11} and G_{21} were set at -10.8 mm Hg, while G_{12} and G_{22} were adjusted to +2.16 mm Hg. These cause transmural pressure changes of -7.5 mm Hg in the upper lobes and +1.5 mm Hg in the lower lobes. Again, main pulmonary arterial and left atrial pressures remained at control values, and pulmonary blood flow rate was allowed to vary in response to system resistance changes.

Results of these simulations are shown in Figures 19 and 20. The changes in mean pressure due to the hydrostatic effects of inertial loadings are apparent: in the upper lobes mean pressure decreases, while it increases in the lower lobes. Deconditioning has little effect on mean lobar pressures, but does introduce changes in the pressure waveshapes on the arterial side; maximum (systolic) pressures are reduced, pulse pressures (maximum minus minimum pressures) are decreased, the secondary (diastolic) peak is much reduced, waveshapes are smoother, and the minimum (diastolic) pressures are highly sensitive to the respiratory cycle (although the minimum diastolic pressure during one respiratory cycle is not much changed by deconditioning). Capillary blood flow waveshapes are also smoother (less pulsatile) in the deconditioned state. These waveshape changes are characteristic of the effects of increased compliance[65].

Changes in transmural pressure due to hydrostatic heads and compliance changes both affect the volume of blood stored in the lungs. As shown in Figure 20, volume in the lower lobes is increased by both increased inertial loading and deconditioning; the computed blood volume in the left lower lobe under a loading of 3-G_z is about 26 ml greater than that during weightlessness.

Perfusion in the lungs is strongly affected by inertial loadings. In a 1-G_z environment, total pulmonary blood flow rate was computed to be about 5 ml/sec (7%) lower than that in the weightless environment, while the decrease was about 18 ml/sec (24%) when the loading increased to 3-G_z; this latter value compares well with the 20% decrease in cardiac output during testing at 3-G_z reported in the literature[49]. Changes in the distribution of perfusion in the lungs are more marked. Blood flow through the upper lobes was decreased by 15 ml/sec (47%) and that through the lower lobes increased by 10 ml/sec (24%) in going from a 0-G_z to a 1-G_z environment. The corresponding figures for a 3-G_z environment are a decrease of 32 ml/sec (100%) in the upper lobes and an increase of 14 ml/sec (33%) in the lower lobes; that is, the model predicts that the upper lobes are totally unperfused at 3-G_z, in agreement with experimental evidence[49,50].

In order to further investigate the effects of a 1-G_z inertial loading on the distribution of blood flow in the lungs, a steady-state model of the pulmonary circulation was formulated. This model is distinct from the model illustrated in Figure 8, but does

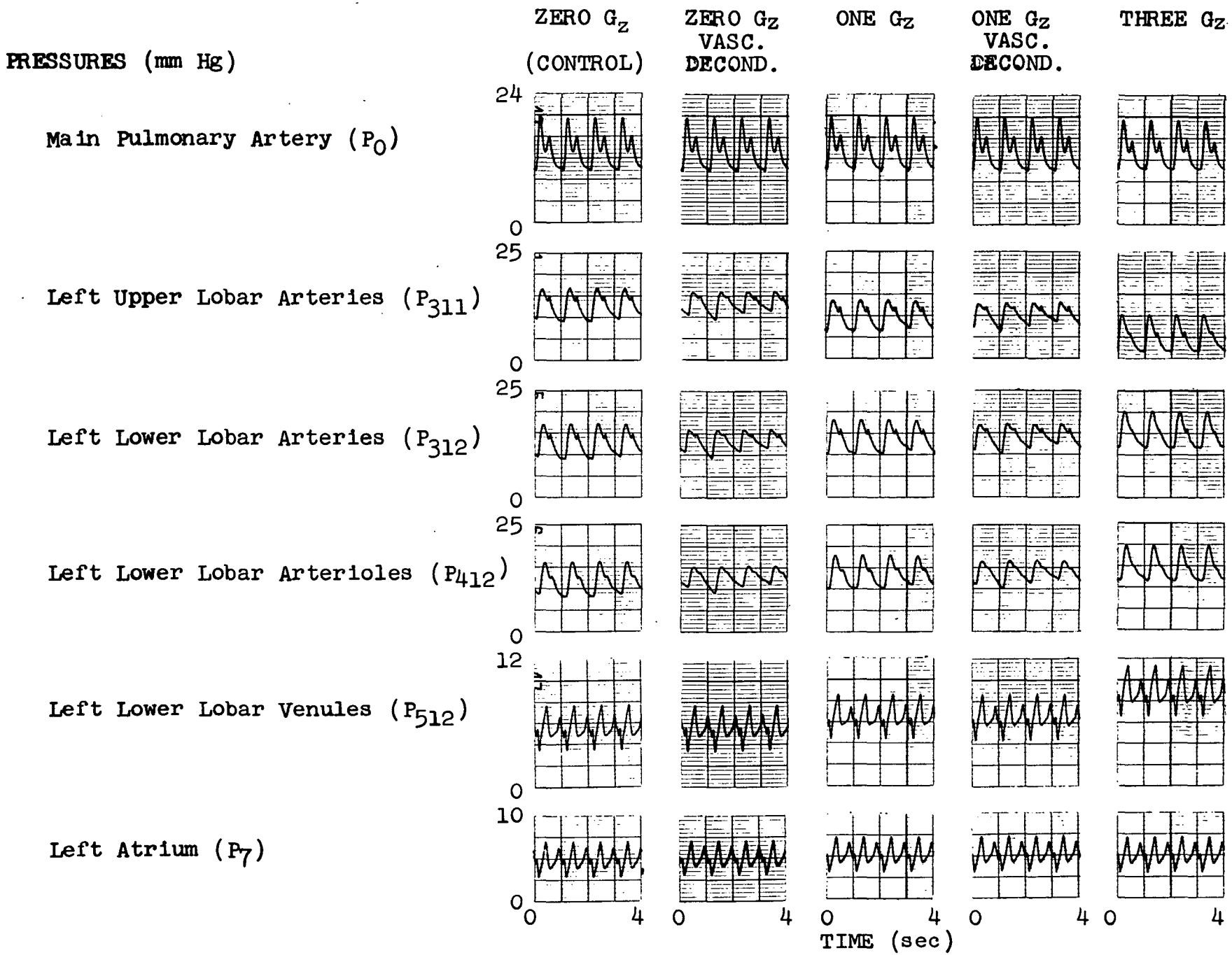

FIGURE 19. SIMULATIONS OF THE EFFECTS OF INERTIAL LOADINGS AND VASCULAR DECONDITIONING - PRESSURES.

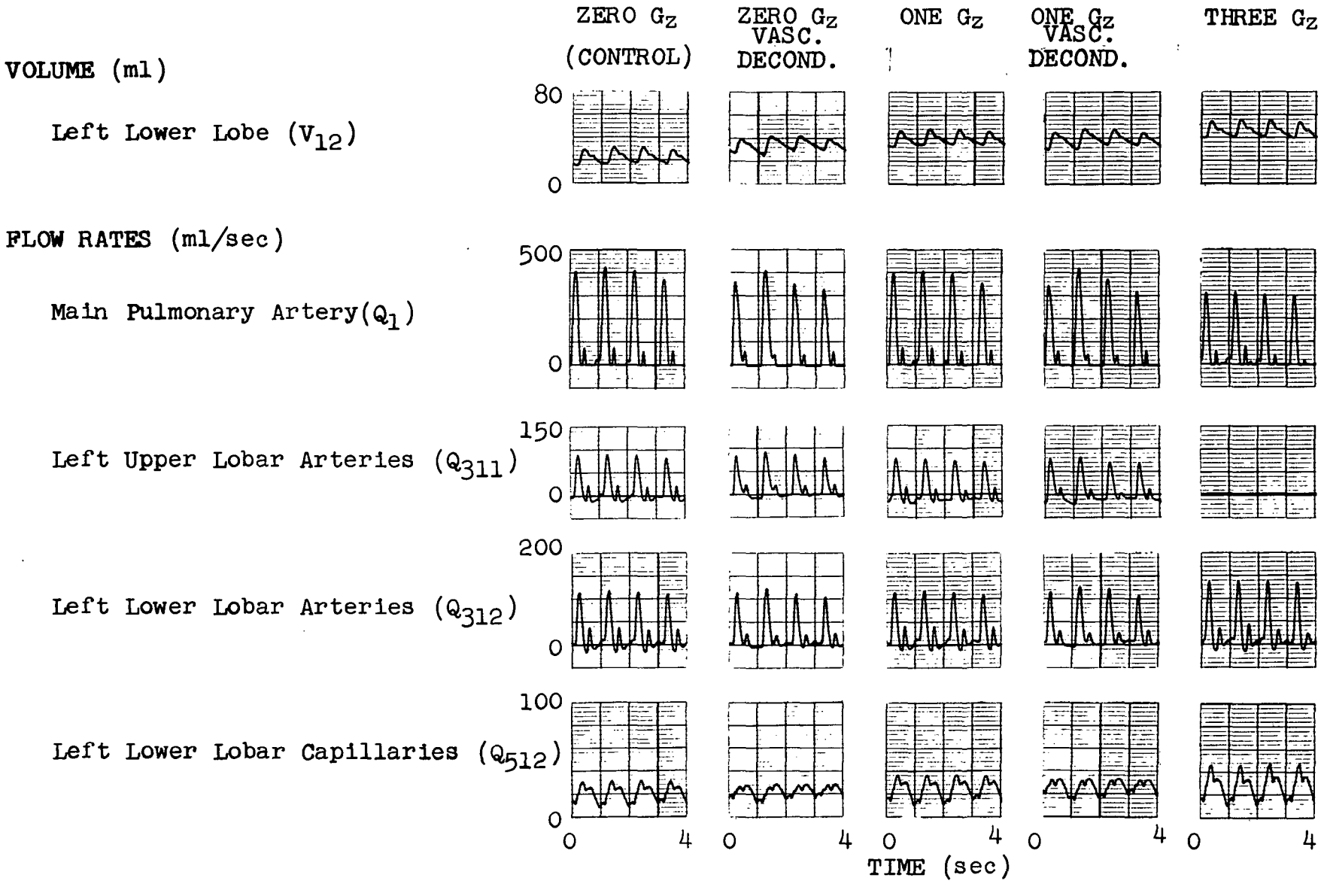

FIGURE 20. SIMULATIONS OF THE EFFECTS OF INERTIAL LOADINGS AND VASCULAR DECONDITIONING - VOLUMES AND FLOW RATES.

use the resistance-transmural pressure relationship shown in Figure 9. It was assumed that the distance between the base and apex of the lung is 30 cm, and that the main pulmonary artery and large pulmonary veins are at the midpoint; that is arterial pressure was assumed to be 15 mm Hg and venous pressure 5 mm Hg at a point 15 cm above the base of the lung. Alveolar pressure was assumed to be zero throughout the lung. Due to hydrostatic heads caused by the inertial loading, transmural pressure varies continuously from apex to base. It was assumed that, correspondingly, vascular resistance also varied continuously from apex to base, in accordance with Figure 9. Driving pressure, on the other hand, is constant throughout the lung since the same hydrostatic heads act on the arterial and venous sides. Blood flow rate, which varies continuously from apex to base in this model, was then computed.

The results (Figure 21) indicate that the flow rate is greatest near the base of the lung and decreases in a non-linear fashion as the distance from the lung base increases. The top 5 cm of the lung are not perfused; the transmural pressure here is so low that the resistance is infinite. The locations of the boundaries between West's three zones[46] (see p. 55) are also shown in Figure 21, assuming a "critical closing pressure" of about 5 mm Hg. The model predictions concerning the distribution of blood flow in the lung in a $1\text{-}G_Z$ field agree quite well with experimental evidence[46,47,49-51]; this gives added confidence in the resistance-transmural pressure relationship used and in the ability of the mathematical model to yield useful predictions concerning the effects of inertial loadings on the pulmonary circulation.

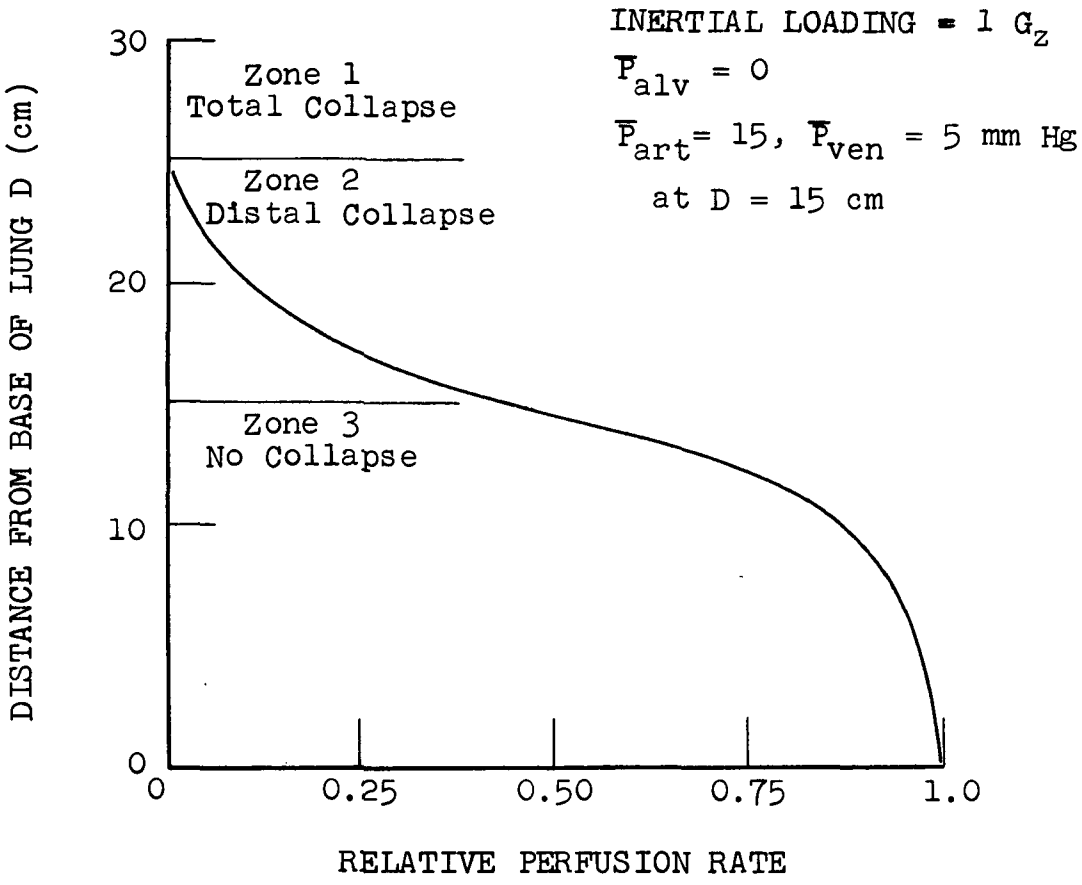

FIGURE 21. MODEL PREDICTION OF TOPOGRAPHICAL DISTRIBUTION OF BLOOD FLOW IN THE LUNG (1 G_z).

Increased Alveolar Pressure

The effects of alveolar pressure on the pulmonary circulation have already been discussed and illustrated in Figure 18. In brief, alveolar pressure is a very important parameter in pulmonary hemodynamics when it is large enough, relative to pulmonary arterial and venous pressures, to cause partial or total collapse or decruitment of the small vessels. The model predicts that increases in alveolar pressure increase the pulmonary vascular resistance, decrease pulmonary blood volume, and decrease pulmonary blood flow rate if arterial and venous pressures are constant. These predictions are in agreement with experimental results taken from isolated lungs. However, if the chest is closed, the situation is somewhat more complex because increased alveolar pressure, such as may be brought about by mechanical positive-pressure respirators, also impedes systemic venous return to the lungs, thus decreasing pulmonary blood flow rate[22]. The model predicts that, as long as the pulmonary blood flow rate is not drastically reduced below normal, the pulmonary arterial pressure will rise slightly during positive-pressure breathing; this tends to minimize the increase in vascular resistance that would occur if alveolar pressure alone increased. The predicted rise in pulmonary arterial pressure during positive-pressure breathing has been observed experimentally[26,62].

Exercise

Muscular exercise has many effects on the cardiovascular system, including an increase in the cardiac output brought about principally by an increase in heart rate. Left atrial pressure changes little

during exercise in a healthy person, but pulmonary arterial pressure is observed to rise by an amount dependent on the level of exercise[26].

In the simulation of exercise, the pulmonary blood flow rate set point $\bar{Q}_1^*$ was increased to 8 l/min, or 3.5 l/min above the control value. Using Fishman's[26] figures that an increase in blood flow rate of about 0.6 to 0.8 l/min is equivalent to an increase of about 100 ml/min in oxygen uptake, the level of exercise simulated matches an oxygen uptake of about 1000 to 1300 ml/min or 500 to 650 ml/min/m^2 BSA based on an average body surface area of 2 square meters. In the simulation, the heart and respiratory rates were kept at their control values, the increased blood flow effectively coming from an increased stroke volume. This is contrary to the behavior of the real system and introduces some errors into the pulsatile portions of the results; however, the mean values of the computed pressures, volumes, and flow rates should not be affected by these errors. The heart and respiratory rates could be altered in the model by changing the input functions, but this was not done in this simulation.

The results of the simulation are shown in Figure 22. Mean pulmonary arterial pressure rose to about 17.2 mm Hg, an increase of about 3.8 mm Hg or 27% above the control value. This result is within the ranges quoted by Comroe[66] and Fishman[26], and agrees very well with Söderholm's empirical equation (quoted by Müller[29]), which yields a mean pulmonary arterial pressure of 17.3 mm Hg for an oxygen uptake of 500 ml/min/m^2 BSA. Pulmonary arterial pressure increases for other levels of pulmonary blood flow rate (i.e., other levels of exercise) are given in Figure 15. Pressure in the venules (P_{512}),

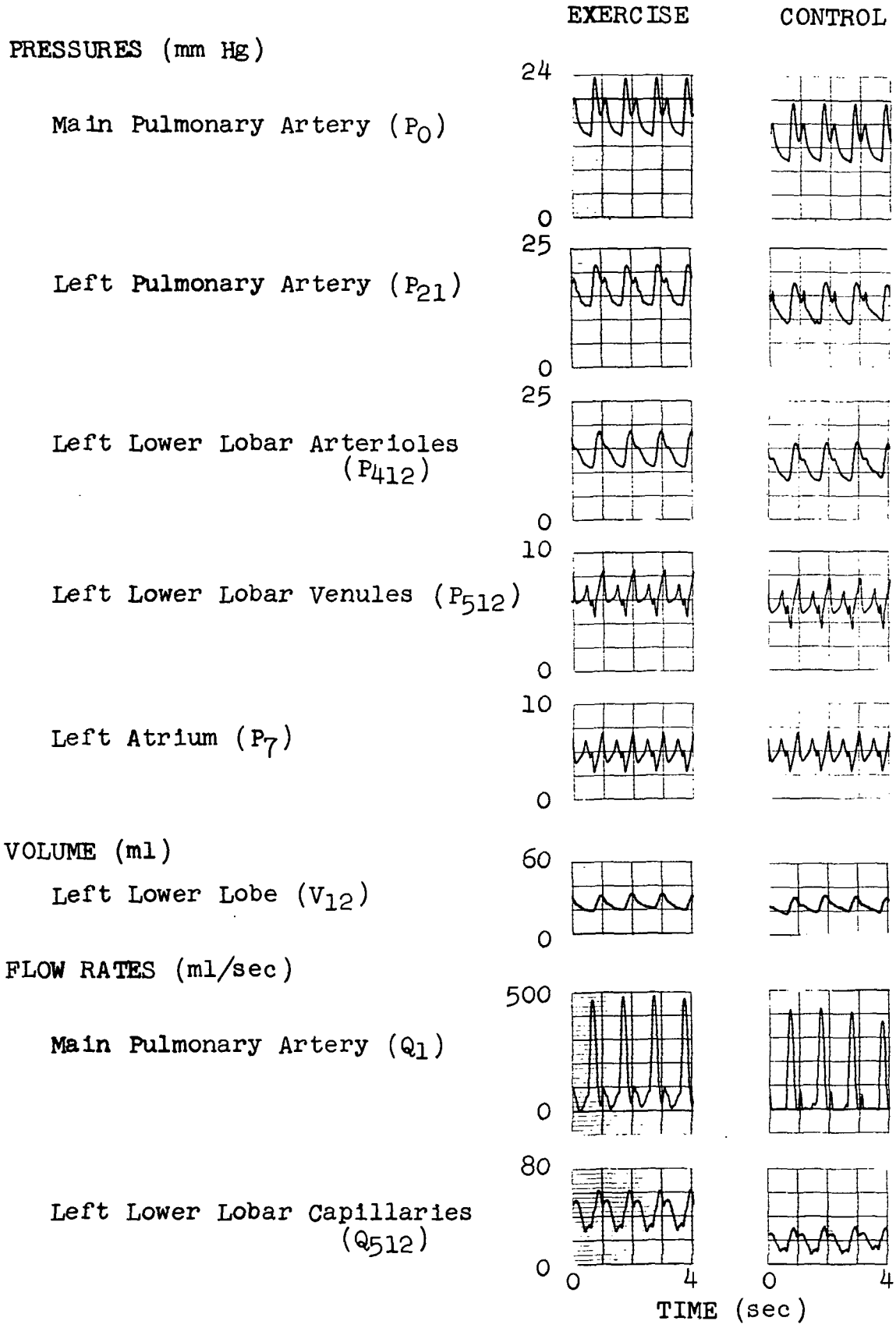

FIGURE 22. SIMULATION OF EFFECTS OF EXERCISE.

which approximates the arterial wedge pressure, rose only by about 1 mm Hg, also in agreement with experimental findings[26].

In the simulation, pulmonary blood volume increased only slightly; the increase is less than indicated by experimental results[25], with the discrepancy perhaps due to the fact that vascular compliance changes were not introduced in the simulation. The predicted mean blood flow rates are accurate, but their waveshapes do not reflect the true effects of exercise because the heart and respiratory rates were not increased in the simulation.

Resistance of the pulmonary vascular bed is decreased significantly during exercise, both in reality[26,62] and in the simulation (in the model, the computed microcirculatory resistances were $R_{511} = 380$, $R_{512} = 254$, $R_{521} = 312$, and $R_{522} = 207$ fluid ohms). Thus, considerable increases in blood flow rate can be accommodated by relatively small increases in pulmonary arterial pressure when cardiopulmonary diseases are absent. An example of the effects of exercise when the lungs are diseased is given below in one of the simulations of interstitial fibrosis.

Acute Hypoxia

Acute hypoxia, or oxygen deficiency caused, for example, by low oxygen partial pressure in the inspired air, has an effect on the pulmonary circulation as well as on the body as a whole. In the lungs, active intrinsic control mechanisms (see p. 7) cause a vasoconstriction in the arterioles or other small vessels[26,52] which increases the resistance and stiffness, but decreases the compliance[67],

of the vascular bed. Left atrial pressure is little affected, but cardiac output increases by up to 30% to 40%[26,67], as the body attempts to transport more oxygen to the tissues.

In the model simulation of hypoxia, the set point for pulmonary blood flow rate $\bar{Q}_1^*$ was increased to 5.4 l/min, 20% above the control value. The vasoconstriction and compliance loss were simulated by assuming that the resistance of the system at the control value of transmural pressure is 300 fluid ohms, double its normal value[22], the resistance versus transmural pressure relationship follows a curve midway between the normal and constant property curves in Figure 9, and the compliances C_{411}, C_{412}, C_{421}, and C_{422} are decreased about 25% to 940 x 10^{-6} fluid farads.

The results of the simulation are shown in Figure 23. The mean pulmonary arterial pressure rose by 7.1 mm Hg to 20.5 mm Hg, an increase of 53%. At this pressure, total vascular resistance was 230 fluid ohms (R_{511} = 1105, R_{512} = 740, R_{521} = 908, and R_{522} = 605 fluid ohms), 53% above the control value. These predicted values compare well with typical measured values, which indicate arterial pressure increases of 4 to 8 mm Hg[26] and resistance increases of about 50%[67] during acute hypoxia. The model predicts a slight increase in pulmonary blood volume, with blood pressure increases overriding the slight loss in system compliance; measurements, however, indicate that while pulmonary capillary blood volume increases in hypoxia, total pulmonary blood volume decreases somewhat[62]. Except for changes in mean values, the differences between the computed pressure and flow waveshapes in the control and hypoxic states appear to be relatively small.

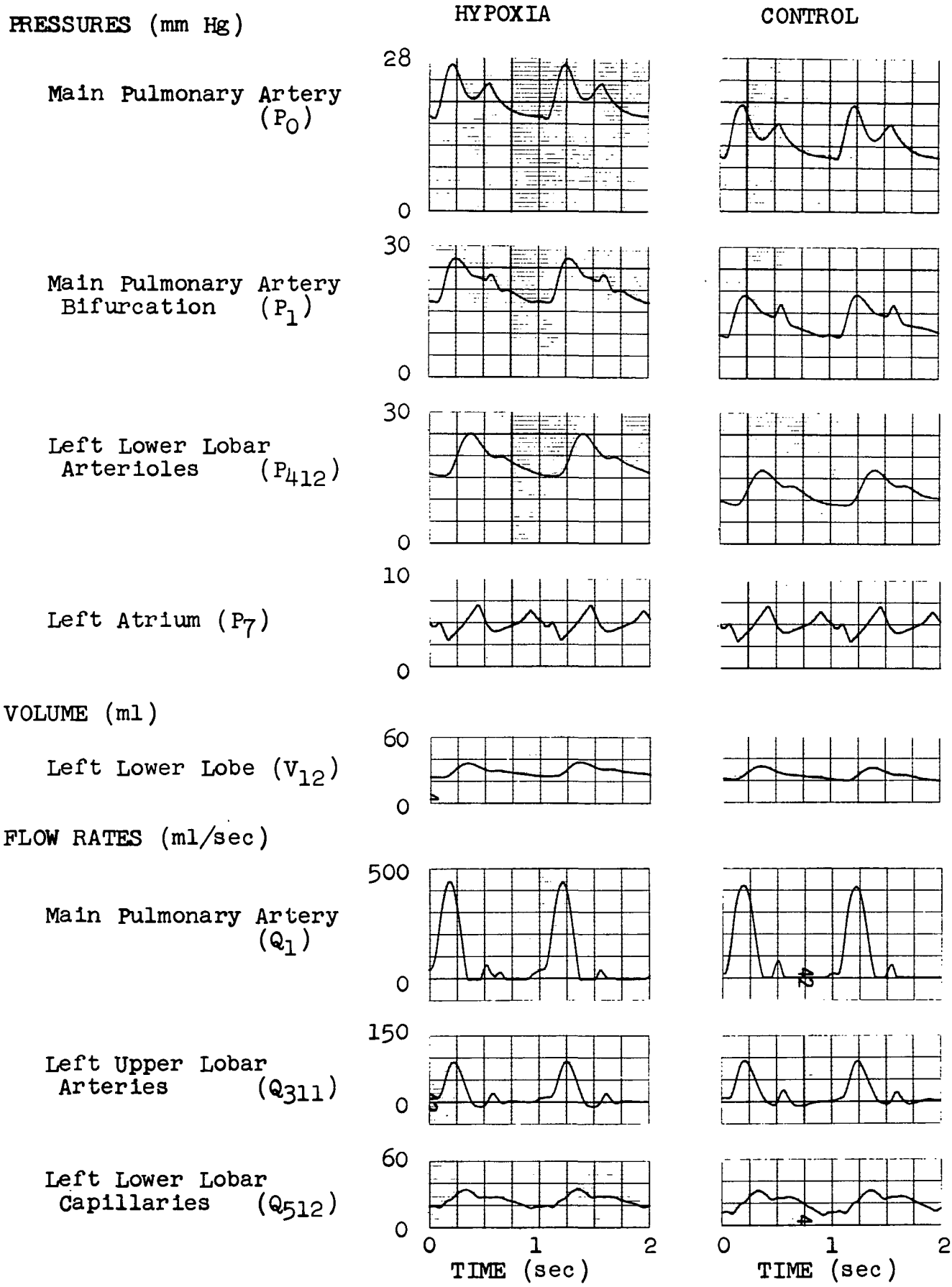

FIGURE 23. SIMULATION OF EFFECTS OF HYPOXIA.

Local and Diffuse Pulmonary Embolism

Embolism refers to the blockage of blood vessels by free-moving blood clots, air bubbles, fat, or other substances. This is a severe problem in the pulmonary circulation, since this vascular bed filters clots formed in the systemic veins, where flow may be sluggish and conducive to clot formation. Important types of pulmonary embolism include the massive clot, which generally lodges in a relatively large vessel, and small but more numerous emboli, which lodge in many of the smaller vessels and produce a diffuse effect.

Local embolism was simulated by assuming that large emboli block 2/3 of the arterial branches in the left lower lobe, so that 2/3 of the effective flow paths are closed below this point. Resistances below this point (R_{412} through R_{712}) then triple, while compliances (C_{412} through C_{612}) are reduced to 1/3 of their control values.

Diffuse embolism, in which 1/2 and 3/4 of the microcirculation is blocked by small numerous emboli, was simulated by increasing the capillary resistances at the control value of transmural pressure by factors of 2 and 4, respectively. At the same time, capillary compliances were reduced; for the case of 1/2 capillary blockage, C_{411}, C_{412}, C_{421}, and C_{422} were reduced to 935 x 10^{-6} fluid farads and C_{511}, C_{512}, C_{521}, and C_{522} to 187 x 10^{-6} fluid farads, while for the case of 3/4 blockage these compliances were reduced to 780 x 10^{-6} fluid farads and 156 x 10^{-6} fluid farads, respectively (here it was assumed that half of the C_{4ij} and C_{5ij} are associated with the capillaries, and these halves were reduced by 1/2 and 3/4, respectively, in the simulations).

Results of the simulations are shown in Figures 24 and 25. The local embolism increased the pulmonary arterial pressure by less than 1 mm Hg, while diffuse blockage of 1/2 of the capillaries caused a rise of only 2.5 mm Hg and blockage of 3/4 of the capillaries caused a rise of only 6.5 mm Hg. These predicted results agree with experimental findings, which indicate that at least 50% to 70% of the cross-section of the vascular bed must be blocked before a significant rise in pulmonary arterial pressure occurs[68,69]. This phenomenon is due to the decrease in vascular resistance as transmural pressure increases, in addition to the increase in driving pressure as arterial pressure rises. Computed values of the microcirculatory resistances at the computed levels of transmural pressure were R_{511} = 576, R_{512} = 1155, R_{521} = 473, and R_{522} = 315 fluid ohms for the case of local embolism, while the respective values were 915, 612, 750, and 500 for diffuse embolism with 1/2 blockage and 1305, 870, 1070, and 715 for diffuse embolism with 3/4 blockage. In the simulations, pressure in the venules, which approximates the arterial wedge pressure, was little changed from the control value, again in agreement with experimental results[69].

The computations indicate that diffuse embolism of up to 75% blockage does not greatly alter the distribution, magnitude, or waveforms of blood flows throughout the lungs. Pressures on the venous side are likewise altered only little from the control state. On the arterial side, however, not only are the mean pressures increased, but the pressure waveforms are also altered. For example, the pulse pressure (maximum minus minimum pressures) is increased.

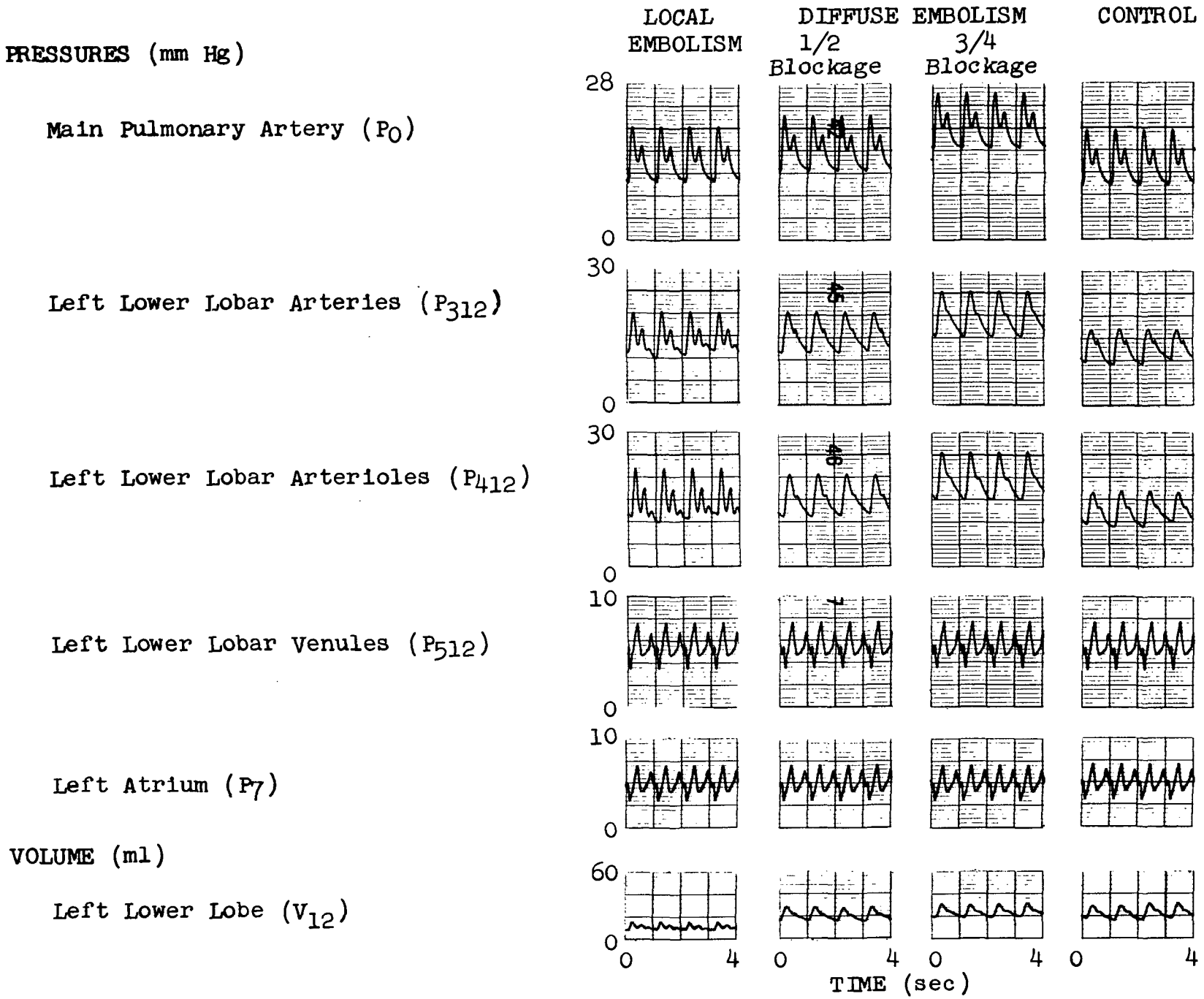

FIGURE 24. SIMULATIONS OF THE EFFECTS OF PULMONARY EMBOLISM - PRESSURES AND VOLUMES.

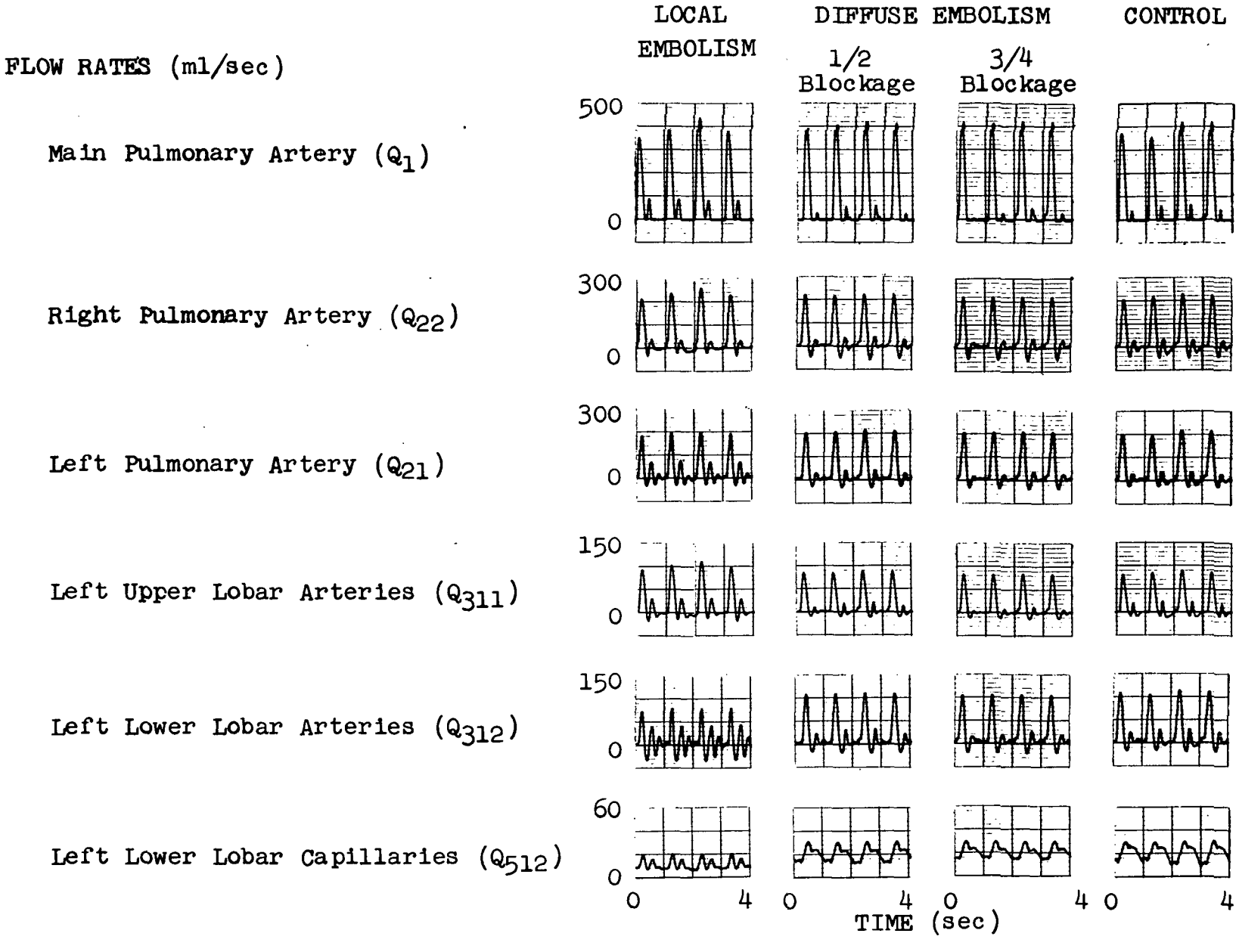

FIGURE 25. SIMULATIONS OF THE EFFECTS OF PULMONARY EMBOLISM - BLOOD FLOW RATES.

This is due to the decrease in damping and increase in wave reflection caused by changes in system resistance and compliance. Blood volume in the lungs remains at about the control value for 1/2 blockage, but increases slightly when 3/4 of the capillaries are blocked; in this latter case the increase in transmural pressure dominates over the loss of vascular compliance.

In local embolism, the changes from the control state are more pronounced, particularly near the site of the blockage (left lower lobar arteries in the simulation). Pressures in the partially blocked lobe (P_{312}, P_{412}) are greatly altered in form due to the large local changes in damping, wave transmission, and reflection characteristics. Blood volume in the blocked lobe is decreased due to the compliance loss. Flows through the partially blocked lobe (Q_{312}, Q_{512}) are decreased strongly and are highly pulsatile. On the other hand, flows through the patent lobe of the left lung (Q_{311}) and the patent right lung (Q_{22}) are increased above the control levels in compensation; these flow pulses have approximately the same waveforms as in the control state.

Excision of the Right Lung

Surgical removal of diseased lung tissue has become prevalent in the treatment of lung cancer and severe tuberculosis. It is important to determine, prior to surgery, the effects of the surgery on the ability of the remaining tissue to oxygenate the blood and on the ability of the right heart to perfuse the remaining pulmonary vascular bed without failing. Often it is difficult to assess these factors because the remaining lung tissue may not be

normal, particularly in older patients. Models of the pulmonary circulation may aid in making this assessment.

As an example, a simulation of the excision of the entire right lung was performed. That is, the flow paths to the right lung were opened at points 1 and 7 in Figure 8. The remaining lung was assumed to have normal compliance and resistance. In view of the physiological evidence[26], pulmonary blood flow rate, heart rate, and left atrial pressure were held at their control values. Thus, the right heart was required to drive the total normal blood flow through one lung alone.

Results are shown in Figures 26 and 27. Main pulmonary arterial pressure rose by about 3.4 mm Hg or 26%, which is close to the 4 mm Hg[70] or 18% to 22%[71] rises found experimentally. Pressures throughout the remaining lung rose correspondingly, while resistance of the left lung dropped to 64% of its control value (R_{511} = 359, R_{512} = 240 fluid ohms) and blood volume in the left lung rose slightly; these results also correspond to the observed behavior[26]. Blood flow rates through the left lung, of course, increased, with almost no backflow occurring in the larger arteries, in contrast to the control state.

Removal of one lung significantly decreases the total compliance of the pulmonary vascular bed[62]. This results in a decrease in the damping of the higher frequency components of the waveforms, as can be seen in the results for P_{312}, P_{412}, and all the computed flow rates. The decreased compliance also causes the appearance of multiple peaks in the Q_1 waveform.

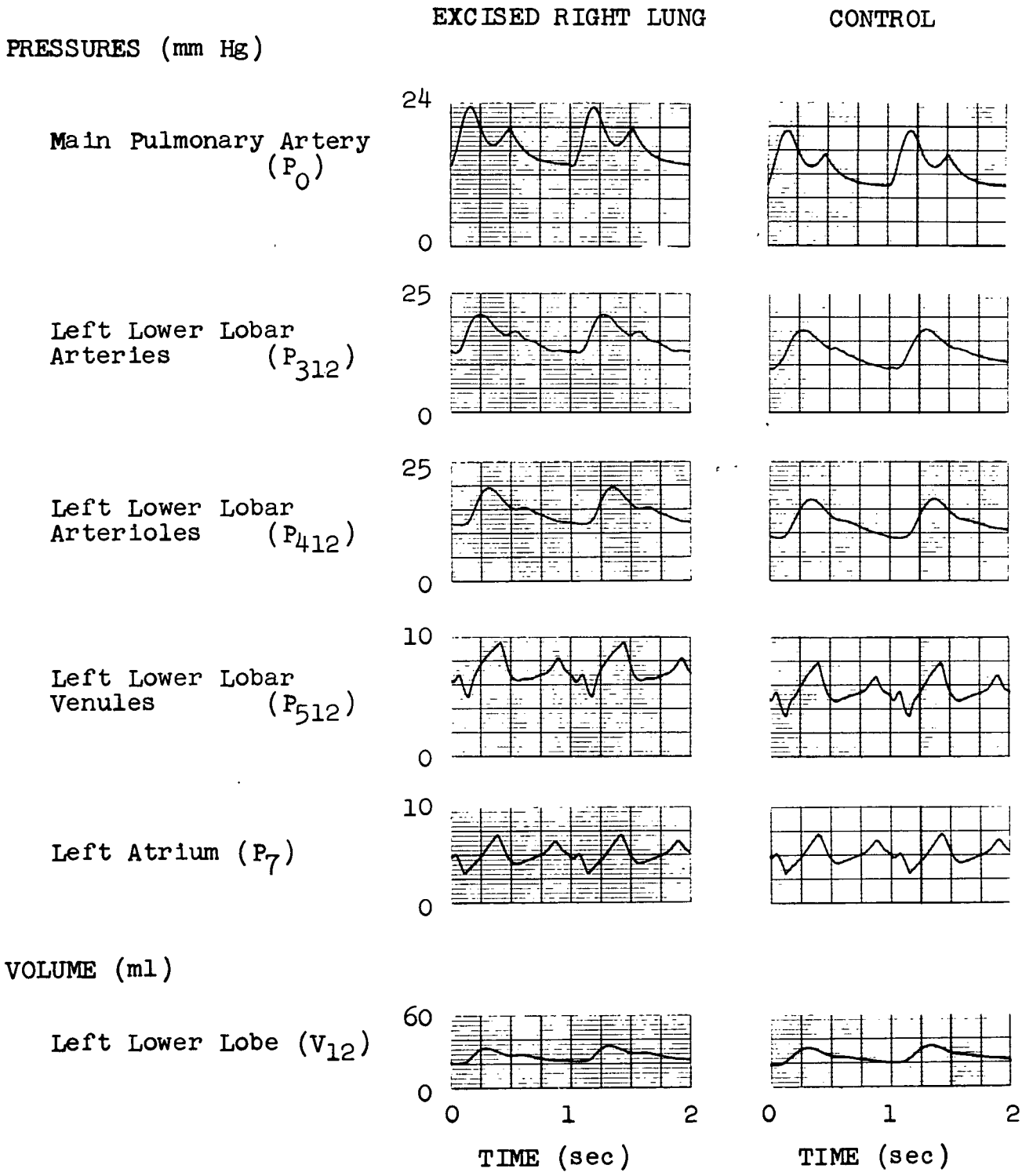

FIGURE 26. SIMULATION OF EXCISION OF THE RIGHT LUNG - PRESSURES AND VOLUMES.

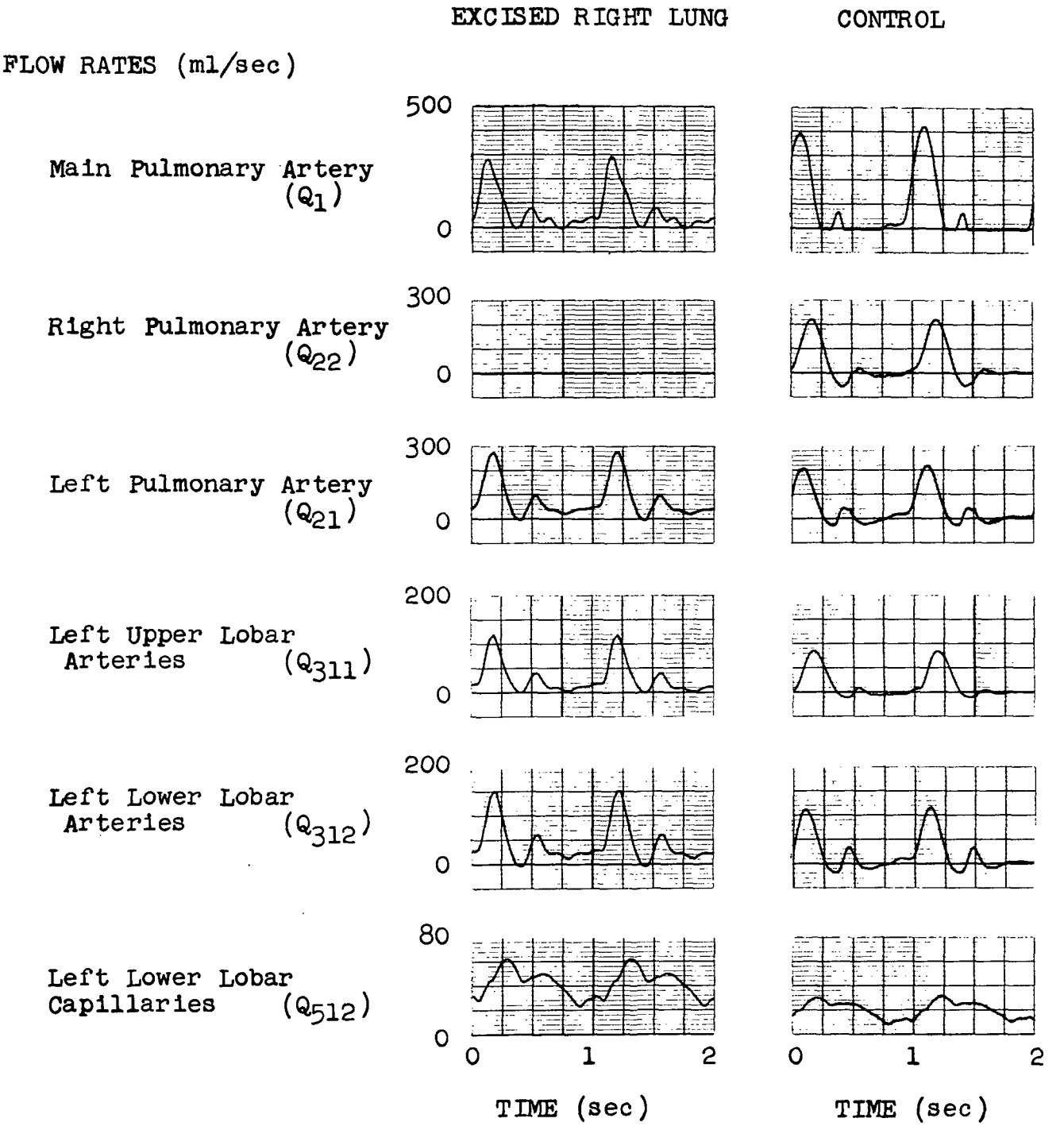

FIGURE 27. SIMULATION OF EXCISION OF THE RIGHT LUNG - BLOOD FLOW RATES.

The predictions of this simulation are in agreement with the physiological findings, and indicate that removal of large amounts of lung tissue leads to relatively small increases in pulmonary arterial pressure if the remaining tissue is healthy and compliant[26,29,66]. Model simulations of the effects of excision when the remaining tissue is abnormal could also be easily performed by varying the resistive and compliant properties of the remaining portions of the model.

Circulatory Shock

Circulatory shock refers to an abnormal state of the cardiovascular system in which the cardiac output is severely reduced from its normal value. Often this results in a corresponding drop in systemic arterial pressure, central venous pressure, and left atrial pressure[22]. Despite these reductions in blood flow rates and pressures, pulmonary arterial pressure has been observed to stabilize at about 2/3 of its normal value[26].

In performing the simulations of circulatory shock, the pulmonary blood flow rate set point $\bar{Q}_1^*$ was lowered successively to 75%, 50%, and 35% of its control value (35% represents the approximate lower limit for survival[22]). At each value of cardiac output, the mean left atrial pressure was lowered in steps of 1 mm Hg from its control value of 5 mm Hg down to 0 mm Hg. These variations in $\bar{Q}_1^*$ and $\bar{P}_7$ bracket the regions of interest in circulatory shock. For each value of cardiac output and left atrial pressure, the mean pulmonary arterial pressure $\bar{P}_0$ required to drive the flow through the system and the total pulmonary vascular resistance were calculated.

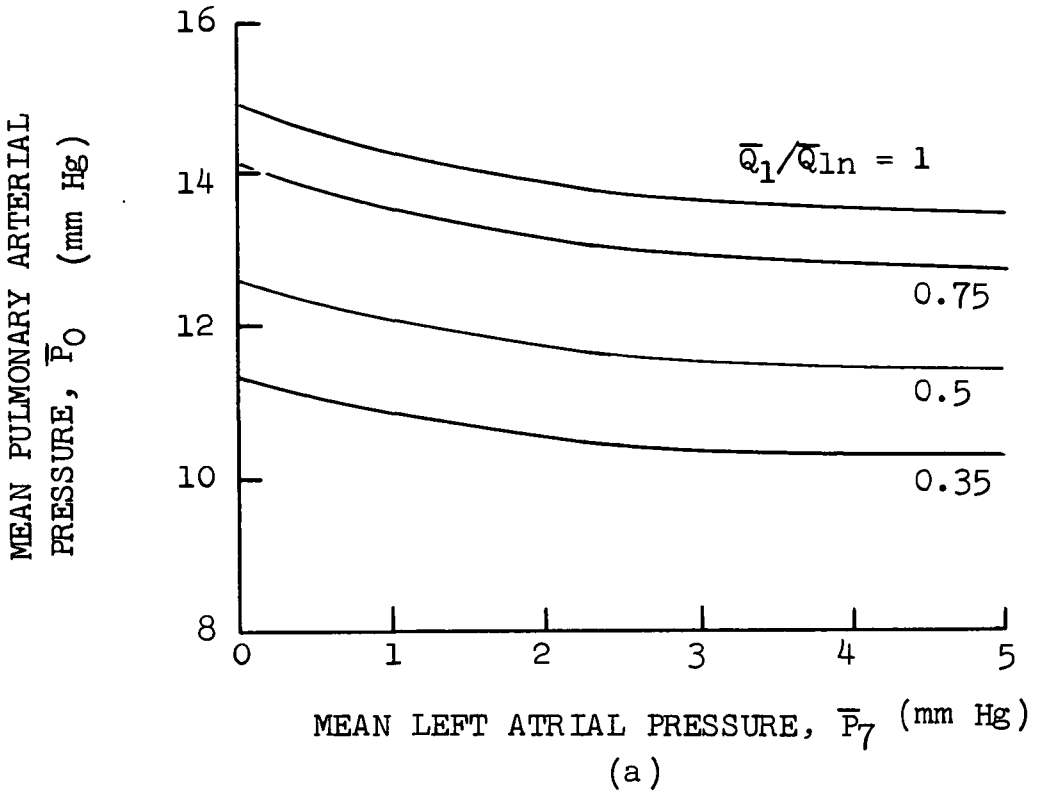

(a)

(b)

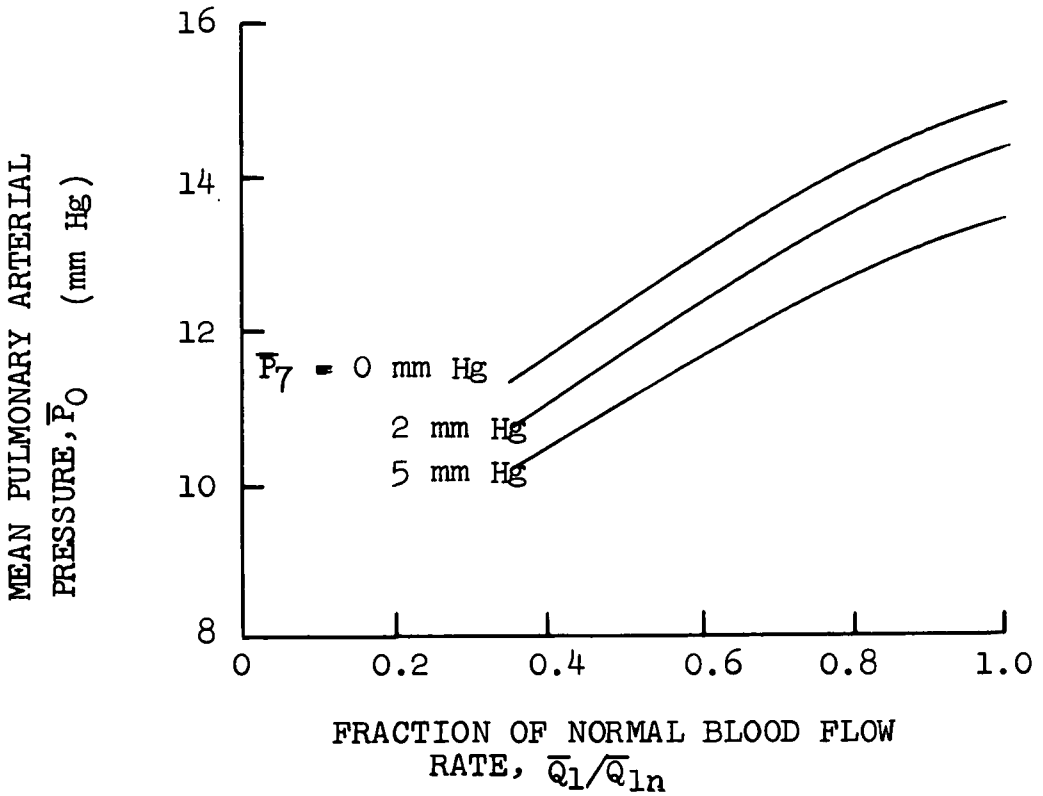

FIGURE 28. SIMULATION OF CIRCULATORY SHOCK.

Results are shown in Figure 28. These clearly illustrate the physiologically observed[26] stabilization (i.e., relatively small changes) of pulmonary arterial pressure despite large changes in cardiac output and left atrial pressure. The model indicates that this stability is due to the increase in pulmonary vascular resistance as the blood pressures drop below normal (Figure 9); resistance increases of up to 3.6 times normal were calculated.

A case of hemorrhagic shock reported in the literature[62] indicated that when pulmonary blood flow fell to 40% of its normal value, the pulmonary vascular resistance tripled and pulmonary arterial pressure dropped by 9%. For a flow rate of 40% of normal, the model predicts similar values, i.e., an increase in resistance to 3.1 times normal and a lowering of arterial pressure by 14%, if left atrial pressure is lowered to 0 mm Hg.

Mitral Stenosis

Mitral stenosis refers to the disease of the mitral valve (which lies between the left atrium and left ventricle) in which the flow of blood from the left atrium is partially obstructed. This obstruction causes a rise in left atrial pressure, the "back pressure" of the pulmonary circulation. In order to maintain the normal cardiac output, the pulmonary arterial pressure must also rise in compensation; that is, the right ventricle must pump against a higher pressure. This rise in pulmonary arterial pressure is known as passive pulmonary hypertension[52]. In some cases, arteriolar spasm

or anatomical changes in the vessels occur in addition; when this occurs, pulmonary vascular resistance increases, compliance decreases, and the level of pulmonary arterial pressure must rise still further[26,52,62].

The simulation of mitral stenosis was performed without including the reactive spasm or anatomical vascular changes that occur in some patients. It was assumed that the mean left atrial pressure rose to 25 mm Hg, an increase of 20 mm Hg. The pulmonary blood flow rate set point $\bar{Q}_1^*$ remained at the control value.

The results, shown in Figure 29, indicate that the mean pulmonary arterial pressure must rise to 28 mm Hg, an increase of 14.5 mm Hg above the control value. Arteriolar pressure (P_{412}) also increases by about 15 mm Hg. These results agree with the findings that pulmonary arterial and microcirculatory pressures rise in uncomplicated mitral stenosis, but not to the same degree as the left atrial pressure[26]. Pulmonary vascular resistance is lower than in the control state (R_{511} = 161, R_{512} = 108, R_{521} = 132, R_{522} = 88 fluid ohms) and pulmonary blood volume is increased because of the increase in transmural pressure; both of these predictions are in agreement with information in the literature for mitral stenosis without reactive changes[26]. It should be noted that some published data for mitral stenosis[24] indicate much higher levels of pulmonary arterial pressure than predicted by the model, for equivalent blood flow rates and left atrial pressures. These data probably apply to cases in which reactive vascular changes or

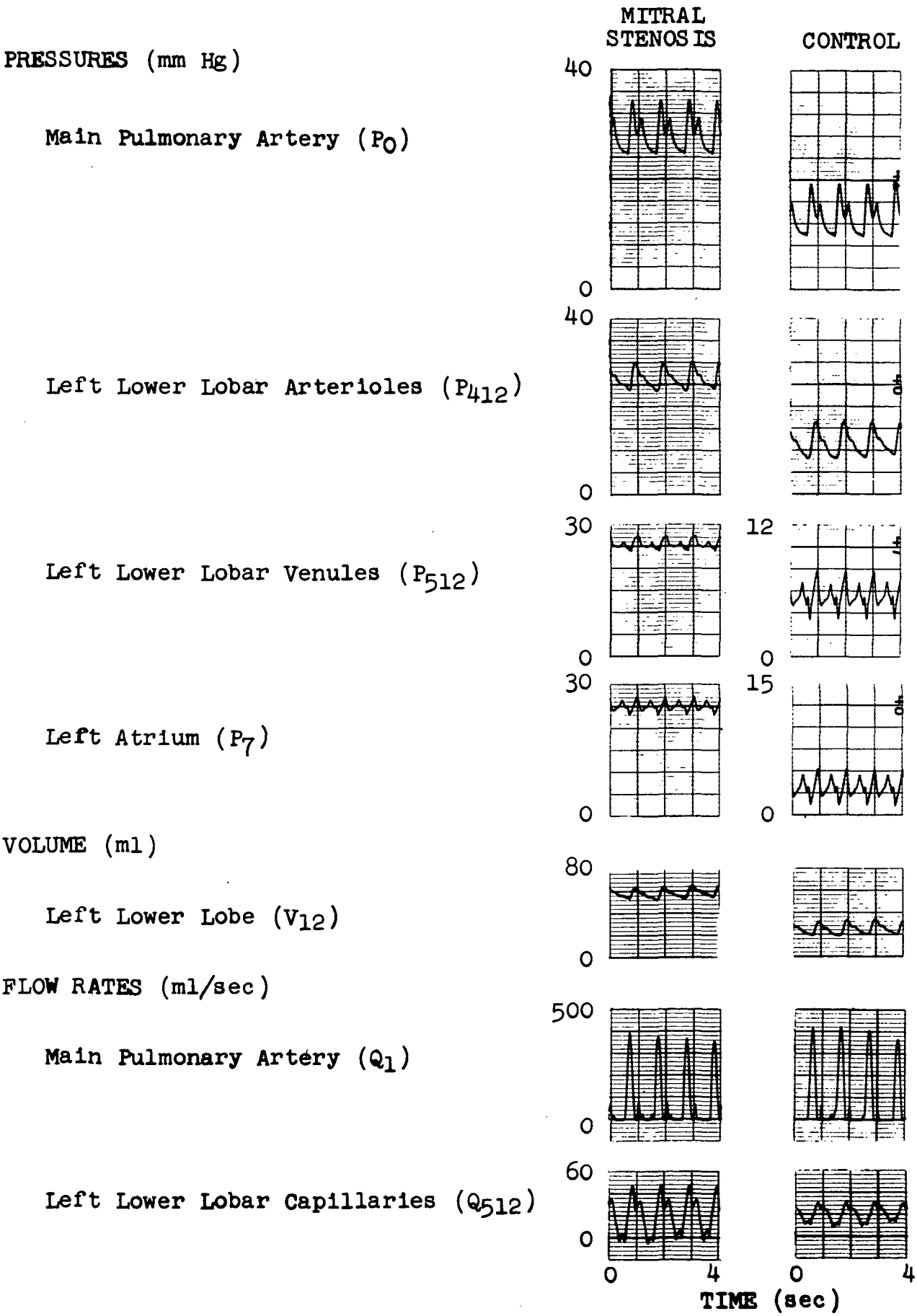

FIGURE 29. SIMULATION OF MITRAL STENOSIS.

arteriolar spasm have increased the vascular resistance sharply, thus causing additional pulmonary hypertension.

Although the mean capillary blood flow rate (Q_{512}) is unchanged from the control valve, the computed waveform in mitral stenosis is more highly pulsatile. This is due to the fact that the mean driving pressure in the mitral stenosis simulation is less than 1/3 that in the control state, while the oscillatory portion of the driving pressure is unchanged; thus, the total driving pressure is more highly pulsatile in the case of mitral stenosis.

Atrial Septal Defect (Left to Right Shunt)

The atrial septal defect, in which an opening exists between the left and right atria, is a common type of congenital heart defect. A portion of the blood passing through the pulmonary circulation thus flows immediately back to the right heart without traversing the left ventricle and systemic circulation. However, the normal systemic cardiac output is generally maintained, so that the amount of blood pumped by the right ventricle, which consists of the normal cardiac output plus the blood shunted through the abnormal opening, is greater than normal. If the interatrial opening is large, the shunt flow and hence the pulmonary blood flow rate may be several times the normal cardiac output (i.e., the pulmonary circulation is hyperkinetic). This puts an added strain on the right ventricle. As long as the pulmonary circulation is highly distensible, the higher flow rate can be pumped by only small increases in pulmonary arterial pressure[25]. However, due to chronic effects of either the elevated pressure or elevated flow rate through the lungs, after a

number of years the pulmonary circulation often develops reactive vascular diseases (primarily at the arteriolar level) which increase vascular resistance and decrease compliance, thus leading to considerable pulmonary hypertension. At the same time the right ventricle may become hypertrophied, which increases the resistance to right ventricular filling and hence decreases the magnitude of the shunt flow through the interatrial opening[25,52]. Thus, the atrial septal defect can lead to a wide spectrum of hemodynamic conditions in the pulmonary circulation.

Atrial septal defects with both normal vascular properties and reactive vascular diseases were simulated. In the case with normal properties the pulmonary flow set point $\bar{Q}_1^*$ was set at 16 l/min, which represents a considerable shunt flow of 11.5 l/min in addition to the normal flow rate of 4.5 l/min; other properties (except the variable capillary resistances) remained at control levels. In the simulation which includes reactive vascular changes, it was assumed that increased filling resistance of the right ventricle decreased the shunt flow to 4.5 l/min, so that $\bar{Q}_1^*$ was set at 9 l/min. At the same time, it was assumed that the resistance of the pulmonary circulation at the control value of transmural pressure is 300 fluid ohms, twice the control value, and that due to the greater stiffness of the vascular bed, the resistance versus transmural pressure relationship follows a curve midway between the normal and constant property curves in Figure 9. Compliances C_{411} through C_{422} were also decreased by 25% to 940×10^{-6} fluid farads.

Results of the simulations are shown in Figure 30. In the case with normal vascular properties, mean pulmonary arterial pressure rose to about 22.5 mm Hg, which is within the range of 21 to 23 mm Hg measured in patients with atrial septal defects and pulmonary blood flow rates of 16 to 18 l/min[24]. At this pressure, the microcirculatory resistances were computed to be R_{511} = 228, R_{512} = 152, R_{521} = 187, and R_{522} = 124 fluid ohms, which are below the control values because of the increase in transmural pressure. Pulmonary blood volume increased somewhat, also in agreement with measurements[26,72]. Blood flow rates, of course, are increased considerably (to 3.5 times the normal value) throughout the vascular bed. This simulation shows that relatively large shunt flows can be accommodated by the normal lung with relatively small increases in driving pressure due to the decrease of vascular resistance with increasing transmural pressure.

When reactive vascular changes occur the situation is much different. In this case the mean pulmonary arterial pressure increased to 32 mm Hg, nearly 2.5 times the control value. This increase is much more than occurred in the case of the septal defect with normal lung properties, despite the fact that the blood flow rate is much lower in the simulation with reactive changes; the differences are due to the increase in vascular resistance and the greater vascular stiffness when reactive changes occur (in this case the computed microcirculatory resistances were R_{511} = 1035, R_{512} = 692, R_{521} = 850, and R_{522} = 565 fluid ohms, which are much above the control values despite the increase in transmural pressure).

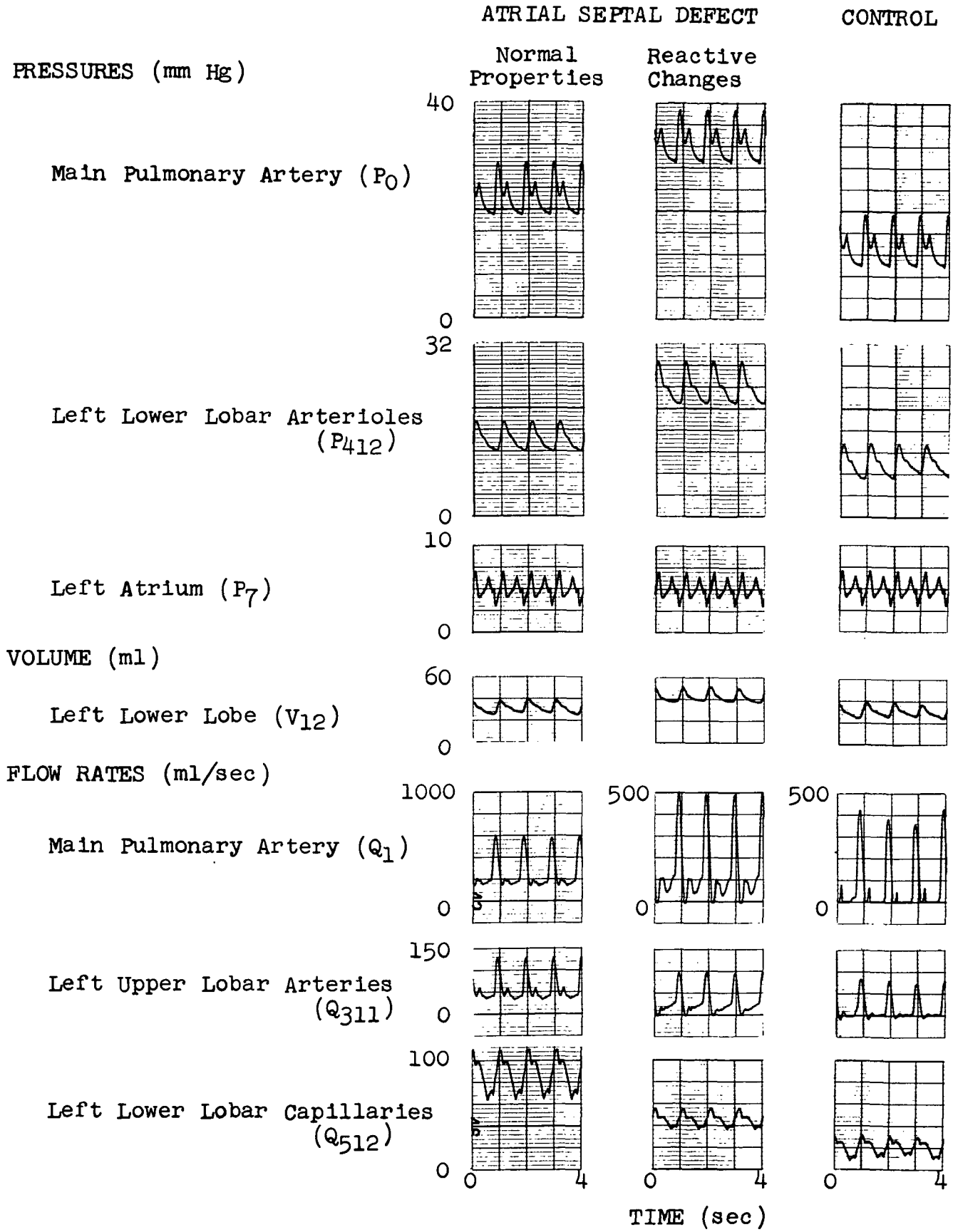

FIGURE 30. SIMULATIONS OF EFFECTS OF ATRIAL SEPTAL DEFECTS, WITH AND WITHOUT REACTIVE VASCULAR CHANGES.

Although the total system compliance decreased slightly in the simulation, the pulmonary blood volume increased considerably above the control value because of the much greater transmural pressure. Blood flow rates are all twice the control values and are also somewhat different in waveshape from the control state.

Emphysema and Interstitial Fibrosis

Emphysema and interstitial fibrosis are diseases of the lungs which affect both ventilation and perfusion. In emphysema, many of the alveolar walls are destroyed; since these walls contain the pulmonary capillaries, their destruction obliterates the small vessels and hence raises vascular resistance and lowers vascular compliance. In addition, since emphysema also diminishes ventilation, some of the alveoli become hypoxic, leading to vasoconstriction and a further increase in vascular resistance. The hypoxia leads to some increase in cardiac output. This combination of factors leads to chronic pulmonary hypertension which often overloads the right heart, causing death[22,52].

Interstitial fibrosis refers to the development of stiff, fibrous tissue in the lungs. This tissue surrounds the blood vessels, which lose their ability to expand; that is, the compliance of the vascular bed diminishes. Although this does not necessarily affect perfusion at rest, the inability of the vessels to dilate often causes high levels of pulmonary hypertension during exercise[22,62].

In the simulation of emphysema, the capillary resistances at the control value of transmural pressure were assumed to be triple the control values, due to both obliteration and hypoxic vaso-constriction, and the resistance versus transmural pressure relation

was assumed to lie midway between the normal and constant property curves in Figure 9; the compliances C_{411} through C_{422} were reduced to 625 x 10^{-6} fluid farads, while C_{511} through C_{522} were reduced to 187 x 10^{-6} fluid farads. To account for the increased cardiac output due to hypoxia, the pulmonary blood flow rate set point $\bar{Q}_1^*$ was raised to 5 l/min.

Since interstitial fibrosis primarily decreases compliance, this disease was simulated by decreasing the compliances C_{411} through C_{422} to 312 x 10^{-6} fluid farads, 1/4 of their control values. Due to the rigidization of the vascular bed, it was then assumed that the resistance versus transmural relation followed a curve lying between the normal and constant property curves in Figure 9, and 1/4 of the distance from the constant property line. At rest, the pulmonary blood flow rate was set at the control value, while in the simulation of exercise $\bar{Q}_1^*$ was increased to 8 l/min or 3.5 l/min above the control value.

Results of the simulations are given in Figures 31 and 32. For emphysema, the model predicts a mean pulmonary arterial pressure of about 22.8 mm Hg, a rise of 9.4 mm Hg. This is within the range of mean arterial pressures quoted by some sources[24], but not as high as the figures given by Müller[29]. Computed pulmonary blood volume dropped to less than half of the control value, close to the experimental result[73]. Resistance of the vascular bed was nearly double the control value, with computed microcirculatory resistances being R_{511} = 1375, R_{512} = 920, R_{521} = 1125, and R_{522} = 750 fluid ohms.

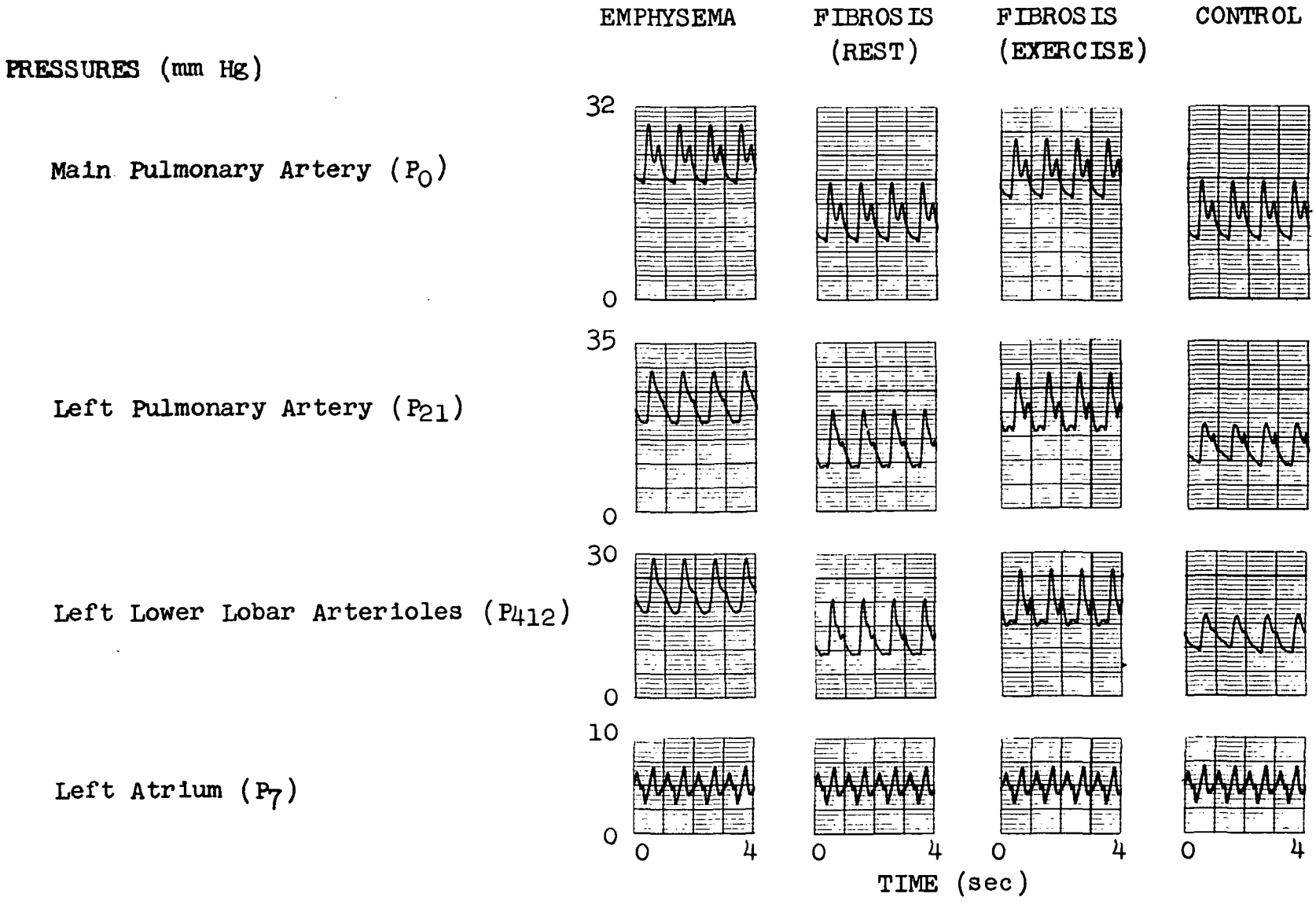

FIGURE 31. SIMULATIONS OF THE EFFECTS OF EMPHYSEMA AND INTERSTITIAL FIBROSIS DURING REST AND EXERCISE - PRESSURES.

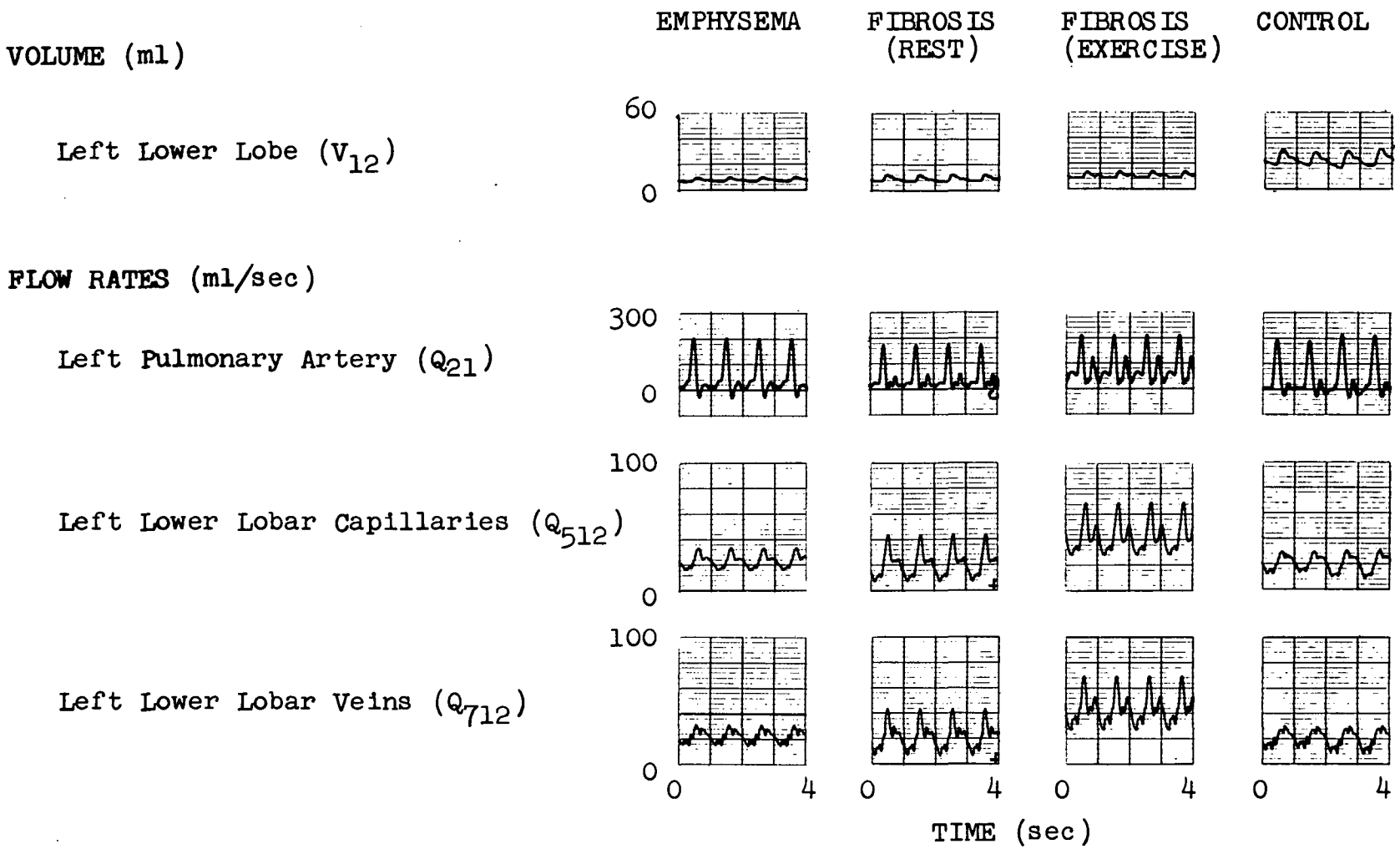

FIGURE 32. SIMULATIONS OF THE EFFECTS OF EMPHYSEMA AND INTERSTITIAL FIBROSIS DURING REST AND EXERCISE - VOLUMES AND FLOW RATES.

The predicted decrease in pulmonary blood volume in interstitial fibrosis has also been observed[73]. The simulations indicate that, at rest, fibrosis has very little effect on the mean pressures in the pulmonary circulation, but exercise causes relatively large arterial pressure increases. The mean arterial pressure in the simulation with fibrosis increased by about 7.1 mm Hg, compared to a computed increase of only 2.5 mm Hg at the same blood flow rate when fibrosis was absent. The computed arterial pressure rise of 7.1 mm Hg is very close to a measured rise of 6 mm Hg during exercise with a similar cardiac output of 8.4 l/min[74]. At rest, the vascular resistance was the same as in the control state, while during exercise the computed microcirculatory resistances were $R_{511} = 565$, $R_{512} = 378$ $R_{521} = 465$, and $R_{522} = 310$ fluid ohms.

The severe changes in resistances and compliances in emphysema and interstitial fibrosis decrease the damping and increase wave reflection in the pulmonary vascular bed. This is seen in the increased pulse pressures on the arterial side as well as in the distinctive waveshapes of pressures and flow rates (in particular P_{21}, P_{412}, Q_{512}, and Q_{712}). If means were available for measuring these quantities <u>in vivo</u>, these distinctive waveshapes could be of diagnostic value.

V. CONCLUSIONS

Based on the physical sciences of fluid and solid mechanics, a mathematical model for the mechanics of the pulmonary circulation has been developed. By focusing on the physical mechanisms which operate in the body, this approach can be useful in addressing current problems of interest in environmental physiology and clinical medicine.

A lumped-parameter approach is used, with the model parameters accounting for the inertial, viscous, and elastic properties of the pulmonary circulation. The form of the model is based on anatomical and physiological data, as well as on the theoretical analysis of the dynamics of unsteady, viscous flow through distensible tubes. Of particular importance is the inclusion in the model of the physiologically observed variation of flow resistance with transmural pressure; this introduces a non-linearity into the model. Also, a control system allows the adjustment of system pressures to meet specified total blood flow rates. Enough detail is included so that information concerning blood pressures, flow rates, and volumes in each important class of vessels (arteries, arterioles, capillaries, venules, and veins) in each lobe of the lungs can be derived.

Solution of the coupled equations describing the model has been accomplished using the electronic analog capability of a hybrid computer. This enables real-time solutions to be obtained and allows great flexibility in varying the many model parameters to simulate interesting situations.

Twenty simulations of the effects of abnormal environments (e.g., space) and pathological conditions have been performed. These have included effects of weightlessness, high inertial loadings, vascular deconditioning, exercise, abnormal alveolar pressure, hypoxia, and examples of obstructive, vasoconstrictive, obliterative, hyperkinetic, and passive pulmonary hypertensive diseases. Model predictions have agreed very well with the available physiological data concerning these abnormal situations. Thus, the model appears to be valid for a wide range of important conditions.

Models of this type, which correctly predict the behavior of the real system during excursions from the normal system operating point, have many applications in environmental physiology and clinical medicine. For example, they can be used as tools for assessing the effects of hazardous environments and for guiding and evaluating space physiology experiments. In medicine, they can be used for training personnel in cardiovascular dynamics, as part of a computer-assisted diagnostics system, and for predicting the results of proposed therapies.

REFERENCES

1. A. Noordergraaf, "Hemodynamics", Chap. 5 in Biological Engineering, ed. H. Schwan, McGraw-Hill, New York, 1969, pp. 391-545.

2. R. Skalak, "Wave Propagation in Blood Flow", Biomechanics, ed. Y. Fung, American Society of Mechanical Engineers, New York, 1966, pp. 20-46.

3. J. Womersley, "An Elastic Tube Theory of Pulse Transmission and Oscillatory Flow in Mammalian Arteries", TR 56-614, Wright Air Development Center, Ohio, 1957.

4. H. Atabek and H. Lew, "Wave Propagation Through a Viscous Incompressible Fluid Contained in an Initially Stressed Elastic Tube", Biophysical Journal, Vol. 6, 1966, pp. 481-503.

5. R. Cox, "Comparison of Linearized Wave Propagation Models for Arterial Blood Flow Analysis", Journal of Biomechanics, Vol. 2, 1969, pp. 251-265.

6. E. Bulanowski and H. Yeh, "Hemodynamic Flow in Anisotropic, Viscoelastic, Thick-Wall Vessels", Journal of Applied Mechanics, Vol. 38, 1971, pp. 351-362.

7. C. Chang and H. Atabek, "The Inlet Length for Oscillatory Flow and Its Effects on the Determination of the Rate of Flow in Arteries", Physics in Medicine and Biology, Vol. 6, 1961, pp. 303-317.

8. N. Kuchar and S. Ostrach, "Unsteady Entrance Flows in Elastic Tubes with Application to the Vascular System", AIAA Journal, Vol. 9, 1971, pp. 1520-1526.

9. J. Lambert, "On the Nonlinearities of Fluid Flow in Non-rigid Tubes", Journal of the Franklin Institute, Vol. 266, 1958, pp. 83-102.

10. M. Anliker, R. Rockwell, and E. Ogden, "Nonlinear Analysis of Flow Pulses and Shock Waves in Arteries, Parts I and II", Zeitschrift für angewandte Mathematik und Physik, Vol. 22, 1971, pp. 217-246 and 563-581.

11. E. Kresch and A. Noordergraaf, "A Mathematical Model for the Pressure-Flow Relationship in a Segment of Vein", IEEE Transactions on Bio-Medical Engineering, Vol. BME-16, 1969, pp. 296-307.

12. R. Whitmore, "A Theory of Blood Flow in Small Vessels", Journal of Applied Physiology, Vol. 22, 1967, pp. 767-771.

13. M. Bloor, "The Flow of Blood in the Capillaries", Physics in Medicine and Biology, Vol. 13, 1968, pp. 443-450.

14. J. Fitz-Gerald, "Mechanics of Red Cell Motion in Very Narrow Capillaries", Proceedings of the Royal Society, London, Series B, Vol. 174, 1969, pp. 193-227.

15. Y. Fung, "Blood Flow in the Capillary Bed", Journal of Biomechanics, Vol. 2, 1969, pp. 353-372.

16. Y. Fung and S. Sobin, "Theory of Sheet Flow in Lung Alveoli", Journal of Applied Physiology, Vol. 26, 1969, pp. 472-488.

17. N. Kuchar, "Studies of the Pulmonary Circulation", Annual Report, NASA Contract NASW-1896, General Electric Company, Philadelphia, May 31, 1970.

18. H. Gray, Anatomy of the Human Body, 27th edition, edited by C. Goss, Lea and Febiger, Philadelphia, 1959.

19. E. Weibel and D. Gomez, "Architecture of the Human Lung", Science, Vol. 137, 1962, pp. 577-585.

20. E. Weibel, Morphometry of the Human Lung, Springer, Berlin, 1963.

21. G. Cumming, R. Henderson, K. Horsfield, and S. Singhal, "The Functional Morphology of the Pulmonary Circulation", in The Pulmonary Circulation and Interstitial Space, edited by A. Fishman and H. Hecht, University of Chicago Press, Chicago, 1969, pp. 327-340.

22. A. Guyton, Textbook of Medical Physiology, 3rd edition, W.B. Saunders, Philadelphia, 1966.

23. J. Greenfield and D. Griggs, "Relation Between Pressure and Diameter in Main Pulmonary Artery of Man", Journal of Applied Physiology, Vol. 18, 1963, pp. 557-559.

24. D. Dittmer and R. Grebe, eds., Handbook of Respiration, W.B. Saunders, Philadelphia, 1958.

25. R. Peters, The Mechanical Basis of Respiration, Little, Brown, and Co., Boston, 1969.

26. A. Fishman, "Dynamics of the Pulmonary Circulation", in Handbook of Physiology, Section 2: Circulation, Vol. II, edited by W. Hamilton and P. Dow, American Physiological Society, Washington, 1963, pp. 1667-1743.

27. A. Fishman and H. Hecht, eds., Pulmonary Circulation and Interstitial Space, University of Chicago Press, Chicago, 1969.

28. P. Harris and D. Heath, Human Pulmonary Circulation, Williams and Wilkins, Baltimore, 1962.

29. C. Müller, Cardiopulmonary Hemodynamics in Health and Disease, C.C. Thomas, Springfield, 1965.

30. J. Widimsky, S. Daum, and H. Herzog, eds., Pulmonary Circulation, Vol. 5 of Progress in Respiration Research, S. Karger, Basel, 1970.

31. G. Lee, "Regulation of the Pulmonary Circulation", British Heart Journal, Vol. 33, 1971, Supplement pp. 15-26.

32. H. Borst, M. McGregor, J. Whittenberger, and E. Berglund, "Influence of Pulmonary Arterial and Left Atrial Pressures on Pulmonary Vascular Resistance", Circulation Research, Vol. 4, 1956, pp. 393-399.

33. S. Carlill, H. Duke, and M. Jones, "Some Observations on Pulmonary Haemodynamics in the Cat", Journal of Physiology, Vol. 136, 1957, pp. 112-121.

34. D. Heiman, S. Rodbard, A. Schaffer, and G. Snider, "Respiratory Factors Affecting Pulmonary Arterial Blood Pressure and Flow Through the Lungs", Journal of Applied Physiology, Vol. 10, 1957, pp. 31-36.

35. J. Banister and R. Torrance, "The Effects of Tracheal Pressure Upon Flow: Pressure Relations in the Vascular Bed of Isolated Lungs", Quarterly Journal of Experimental Physiology, Vol. 45, 1960, pp. 352-367.

36. T. Lloyd and G. Wright, "Pulmonary Vascular Resistance and Vascular Transmural Gradient", Journal of Applied Physiology, Vol. 15, 1960, pp. 241-245.

37. J. Whittenberger, M. McGregor, E. Berglund, and H. Borst, "Influence of State of Inflation of the Lung on Pulmonary Vascular Resistance", Journal of Applied Physiology, Vol. 15, 1960, pp. 878-882.

38. A. Roos, L. Thomas, E. Nagel, and D. Prommas, "Pulmonary Vascular Resistance as Determined by Lung Inflation and Vascular Pressures", Journal of Applied Physiology, Vol. 16, 1961, pp. 77-84.

39. L. Thomas, Z. Griffo, and A. Roos, "Effect of Negative-Pressure Inflation of the Lung on Pulmonary Vascular Resistance", Journal of Applied Physiology, Vol. 16, 1961, pp. 451-456.

40. S. Permutt, B. Bromberger-Barnea, and H. Bane, "Alveolar Pressure, Pulmonary Venous Pressure, and the Vascular Waterfall", Medicina thoracalis, Vol. 19, 1962, pp. 239-260.

41. J. Mead and J. Whittenberger, "Lung Inflation and Hemodynamics", in Handbook of Physiology, Section 3: Respiration, Vol. I, edited by W. Fenn and H. Rahn, American Physiological Society, Washington, 1964, pp. 477-486.

42. R. Karp, P. Graf, and J. Nadel, "Regulation of Pulmonary Capillary Blood Volume by Pulmonary Arterial and Left Atrial Pressures", Circulation Research, Vol. 22, 1968, pp. 1-10.

43. E. Selkurt, ed., Physiology, 2nd edition, Little, Brown, and Co., Boston, 1966.

44. P. Dejours, Respiration, Oxford University Press, New York, 1966.

45. J. Mead and E. Agostini, "Dynamics of Breathing", in Handbook of Physiology, Section 3, Respiration, Vol. I, edited by W. Fenn and H. Rahn, American Physiological Society, Washington, 1964, pp. 411-427.

46. J. West, "Topographical Distribution of Blood Flow in the Lung", in Handbook of Physiology, Section 3: Respiration, Vol. II, edited by W. Fenn and H. Rahn, American Physiological Society, Washington, 1964, pp. 1437-1451.

47. J. West, "Pulmonary Blood Flow with Special Reference to the Influence of the Space Environment", AIAA Paper No. 70-785, 1970.

48. J. Billingham, "The Effect of Gravity on the Cardiovascular and Respiratory Systems" in Fluid Dynamics of Blood Circulation and Respiratory Flow, AGARD Conference Proceedings No. 65, 1970, pp. 7-1 to 7-5.

49. D. Glaister, "Effects of Acceleration on Pulmonary Blood Flow", in The Pulmonary Circulation and Interstitial Space, edited by A. Fishman and H. Hecht, University of Chicago Press, Chicago, 1969, pp. 391-408.

50. D. Glaister, "Gravity Dependence of Pulmonary Capillary Blood Flow", in Fluid Dynamics of Blood Circulation and Respiratory Flow, AGARD Conference Proceedings No. 65, 1970, pp. 8-1 to 8-8.

51. J. Hogg, P. Holst, P. Corry, F. Ruff, E. Housley and E. Morris, "Effect of Regional Lung Expansion and Body Position on Pulmonary Perfusion in Dogs", Journal of Applied Physiology, Vol. 31, 1971, pp. 97-101.

52. A. Selzer, The Heart: Its Function in Health and Disease, University of California Press, Berkeley, 1969.

53. A. Eringen, Non-Linear Theory of Continuous Media, McGraw-Hill, New York, 1962.

54. N. Kuchar and S. Ostrach, "A Thick-Walled Viscoelastic Model for the Mechanics of Arteries", Journal of Biomechanics, Vol. 2, 1969, pp. 443-454.

55. V. Rideout and D. Dick, "Difference-Differential Equations for Fluid Flow in Distensible Tubes", IEEE Transactions on Bio-Medical Engineering, Vol. BME-14, 1967, pp. 171-177.

56. N. Westerhof, F. Bosman, C. DeVries, and A. Noordergraaf, "Analog Studies of the Human Systemic Arterial Tree", Journal of Biomechanics, Vol. 2, 1969, pp. 121-143.

57. G. Jager, N. Westerhof, and A. Noordergraaf, "Oscillatory Flow Impedance in Electrical Analog of Arterial System", Circulation Research, Vol. 16, 1965, pp. 121-133.

58. M. Snyder and V. Rideout, "Computer Simulation Studies of the Venous Circulation", IEEE Transactions on Bio-Medical Engineering, Vol. BME-16, 1969, pp. 325-334.

59. F. Wiener, E. Morkin, R. Skalak, and A. Fishman, "Wave Propagation in the Pulmonary Circulation", Circulation Research, Vol. 19, 1966, pp. 834-850.

60. G. Pollack, R. Reddy, and A. Noordergraaf, "Input Impedance, Wave Travel, and Reflections in the Human Pulmonary Arterial Tree: Studies Using an Electrical Analog", IEEE Transactions on Bio-Medical Engineering, Vol. BME-15, 1968, pp. 151-164.

61. V. Rideout and J. Katra, "Computer Simulation Study of the Pulmonary Circulation", Simulation, Vol. 12, 1969, pp. 239-245.

62. D. Aviado, The Lung Circulation (2 vols.), Pergamon Press, Oxford, 1965.

63. E. Kennen, A. Stankus, and P. Yu, "Pulmonary Venous Blood Flow Characteristics", Proceedings of the Annual Conference on Engineering in Medicine and Biology, Vol. 9, 1967, p. 167.

64. H. Hultgren and M. Flamm, "Pulmonary Edema", Modern Concepts of Cardiovascular Disease, Vol. 38, 1969, pp. 1-6.

65. S. Reuben, "Compliance of the Human Pulmonary Arterial System in Disease", Circulation Research, Vol. 29, 1971, pp. 40-50.

66. J. Comroe, Physiology of Respiration, Year Book Medical Publishers, Chicago, 1965.

67. S. Reuben, J. Swadling, B. Gersh, and G. Lee, "Impedance and Transmission Properties of the Pulmonary Arterial System", Cardiovascular Research, Vol. 5, 1971, pp. 1-9.

68. F. Gray, "Clinical Physiology of Acute Pulmonary Embolism", in Pulmonary Circulation, Vol. 5 in Progress in Respiration Research, edited by J. Widimsky, S. Daum, and H. Herzog, S. Karger, Basel, 1970, pp. 277-283.

69. J. Hyland, G. Smith, L. McGuire, D. Harrison, F. Haynes, and L. Dexter, "Effect of Selective Embolization of Various Sized Pulmonary Arteries in Dogs", American Journal of Physiology, Vol. 204, 1963, pp. 619-625.

70. J. Rams, R. Harrison, W. Fry, P. Moulder, and W. Adams, "Operative Pulmonary Artery Pressure Measurements as a Guide to Post-Operative Management and Prognosis Following Pneumonectomy, Diseases of the Chest, Vol. 41, 1962, pp. 85-90.

71. V. Ježek, "Pulmonary Hemodynamics in Bronchogenic Cancer Before and After Lung Resection", in Pulmonary Circulation, Vol. 5 in Progress in Respiration Research, edited by J. Widimsky, S. Daum, and H. Herzog, S. Karger, Basel, 1970, pp. 237-243.

72. M. Englert, "Pulmonary Capillary Blood Volume in Conditions With High Pulmonary Blood Flow", in Pulmonary Circulation, Vol. 5 in Progress in Respiration Research, edited by J. Widimsky, S. Daum, and H. Herzog, S. Karger, Basel, 1970, pp. 338-345.

73. R. Backmann and W. Hartung, "Differentiating Measurements of Blood Volumes in Isolated Human Lungs", in Pulmonary Circulation, Vol. 5 in Progress in Respiration Research, edited by J. Widimsky, S. Daum, and H. Herzog, S. Karger, Basel, 1970, pp. 327-337.

74. R. Riley, A. Himmelstein, H. Motley, H. Weiner, and A. Cournand, "Studies of the Pulmonary Circulation at Rest and During Exercise in Normal Individuals and in Patients With Chronic Pulmonary Disease", American Journal of Physiology, Vol. 152, 1948, pp. 372-382.